Neurobiology of Disease 158 (2021) 105474

Contents lists available at ScienceDirect

Neurobiology of Disease

journal homepage: www.elsevier.com/locate/ynbdi

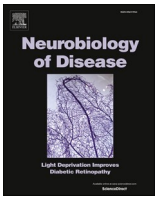

Oxidized/deamidated-ceruloplasmin dysregulates choroid plexus epithelial cells functionality and barrier properties *via* RGD-recognizing integrin binding

Alan Zanardi [a], Marco Barbariga [a], Antonio Conti [a], Franco Vegliani [a], Flavio Curnis [b], Massimo Alessio [a,*]

[a] *Proteome Biochemistry, IRCCS-Ospedale San Raffaele, 20132 Milan, Italy*
[b] *Tumor Biology and Vascular Targeting, IRCCS-Ospedale San Raffaele, 20132 Milan, Italy*

ARTICLE INFO

Keywords:
Ceruloplasmin
Choroid plexus
Blood-cerebrospinal fluid barrier
NGR and *iso*DGR motifs
Deamidation
Oxidation
Secretome
Neurodegeneration
Cerebrospinal fluid
Parkinson's disease

ABSTRACT

Choroid plexus epithelial cells (CPEpiCs) determine the composition of cerebrospinal fluid (CSF) and constitute the blood-CSF barrier (BCSFB), functions that are altered in neurodegenerative diseases. In Parkinson's disease (PD) the pathological environment oxidizes and deamidates the ceruloplasmin, a CSF-resident ferroxidase, which undergoes a gain of RGD-recognizing integrin binding property, that may result in signal transduction. We investigated the effects that oxidized/deamidated ceruloplasmin (Cp-ox/de) may exert on CPEpiCs functions. Through RGD-recognizing integrins binding, Cp-ox/de mediates CPEpiCs adhesion and intracellular signaling, resulting in cell proliferation inhibition and alteration of the secretome profile in terms of proteins related to cell-extracellular matrix interaction. Oxidative conditions, comparable to those found in the CSF of PD patients, induced CPEpiCs barrier leakage, allowing Cp-ox/de to cross it, transducing integrins-mediated signal that further worsens BCSFB integrity. This mechanism might contribute to PD pathological processes altering CSF composition and aggravating the already compromised BCSFB function.

1. Introduction

The choroid plexus is a convoluted structure facing the brain ventricles, composed of fenestrated blood vessels and a monolayer of specialized epithelial cells (Johanson et al., 2011). Choroid plexus epithelial cells (CPEpiCs) mainly determine the production and composition of cerebrospinal fluid (CSF) in terms of proteins, organic molecules, metals, and salts content (Marques et al., 2017). This is achieved by the synthesis and release of proteins and metabolites, and by the regulation of barrier permeability (Marques et al., 2017). Indeed, CPEpiCs constitute the blood-CSF barrier (BCSFB), in which the permeability is strictly controlled by the presence of epithelial tight-junctions (Tietz and Engelhardt, 2015). Moreover, CPEpiCs-derived extracellular vesicles and exosomes have been proposed as communication mechanisms able to deliver compounds in the brain parenchyma during inflammation and neurodegeneration (Balusu et al., 2016; Grapp et al., 2013). Changes in choroid plexus anatomy and function are reported in aging and neurodegenerative diseases, such as Parkinson's disease (PD), Alzheimer's disease (AD), and multiple sclerosis (Demeestere et al., 2015; Emerich et al., 2005; Kaur et al., 2016). These alterations include epithelial atrophy and thickness, expression of stress response proteins, mitochondrial induction of apoptosis, reduced CSF synthesis and turnover, altered permeability, and basal lamina thickening (Anthony et al., 2003; Masseguin et al., 2005; Perez-Gracia et al., 2009; Pisani et al., 2012; Serot et al., 1997; Shrestha et al., 2014; Vargas et al., 2010). These alterations are fostered in AD mainly by amyloid-β deposition, but can be promoted by conditions that characterize several neurodegenerative disorders, like iron and copper homeostasis dysfunction and oxidative stress (Brkic et al., 2015; Mesquita et al., 2012; Perez-Gracia et al., 2009; Vargas et al., 2010; Zheng and Monnot,

Abbreviations: AD, Alzheimer's disease; BCSFB, blood-cerebrospinal fluid barrier; Cp, ceruloplasmin; Cp-ox/de, oxidized/deamidated ceruloplasmin; CPEpiCs, choroid plexus epithelial cells; FN-I_5/37 °C, deamidated fifth type I repeat of human fibronectin; HCPEpiCs, human choroid plexus epithelial cells; *iso*DGR, *iso*-Aspartate-Glycine-Arginine; MS, mass spectrometry; MTT, 3-(4,5-dimethylthiazol-2-yl)-2,5- diphenyltetrazolium bromide; NGR, Asparagine-Glycine-Arginine; PD, Parkinson's disease; PIMT, protein L-isoaspartyl methyltransferase RGD, Arginine-Glycine-Aspartate; VN, vitronectin.

* Corresponding author at: Proteome Biochemistry, IRCCS-Ospedale San Raffaele, via Olgettina 58, 20132 Milan, Italy.
E-mail addresses: zanardi.alan@hsr.it (A. Zanardi), conti.antonio@hsr.it (A. Conti), flavio.curnis@hsr.it (F. Curnis), alessio.massimo@hsr.it (M. Alessio).

https://doi.org/10.1016/j.nbd.2021.105474
Received 29 April 2021; Received in revised form 4 August 2021; Accepted 5 August 2021
Available online 10 August 2021

2012). Thus, the alteration of CPEpiCs physiology in neurodegenerative disease patients can lead to BCSFB dysfunction and CSF composition changes, which might reflect and/or contribute to the pathological mechanisms.

The copper-protein ceruloplasmin (Cp) is a ferroxidase enzyme present in the CSF, which contributes to iron homeostasis regulating cellular iron loading and export (Hellman and Gitlin, 2002; Jeong and David, 2003). The absence of Cp's ferroxidase activity, which characterizes the monogenic rare disease aceruloplasminemia, results in neurodegeneration caused by brain iron accumulation (Piperno and Alessio, 2018). Through regulated iron oxidation, the Cp also protects the central nervous system (CNS) from iron-mediated free radicals injury (Ayton et al., 2013; Texel et al., 2008). The CSF's pathological environment from PD and AD patients promotes oxidative modifications of both endogenous Cp and purified Cp spiked within the CSFs (Barbariga et al., 2015, 2014; Olivieri et al., 2011). Cp structural changes occur upon protein oxidation, with consequent release of coordinated copper ions and loss of ferroxidase activity (Barbariga et al., 2014; Olivieri et al., 2011). Cp modifications promote *de novo* gain of integrin-binding properties, following the deamidation of two Asn-Gly-Arg (NGR)-motifs present in the Cp sequence. Converted into the *iso*Asp-Gly-Arg (*iso*DGR), these motifs are then able to bind Arg-Gly-Asp-(RGD)-recognizing integrins (Barbariga et al., 2015, 2014; Corti and Curnis, 2011; Curnis et al., 2006). The oxidized/deamidated-Cp (Cp-ox/de) transduces *via iso*DGR/integrin binding an intracellular signal that may regulate cell cycle, proliferation, and cytoskeletal rearrangement in epithelial cells (Barbariga et al., 2015, 2014). This signaling results in proliferation inhibition, cell cycle arrest, and apoptosis induction in HaCaT cells, promoting inhibition of CPEpiCs proliferation (Barbariga et al., 2020). *In vivo*, Cp oxidation and deamidation could be fostered by hydrogen peroxide (H_2O_2) found at higher concentrations in the CSF of PD, compared to the CSF of healthy subjects ($\approx$ 50 *vs.* 22 μM, respectively) (Barbariga et al., 2015).

Based on the observations that histological organization, tight junctions and barrier permeability of CPEpiCs are altered in neurodegenerative diseases and on the direct contact of these cells with the CSF, we hypothesized that CPEpiCs could be targeted by Cp-ox/de present in the pathological CSF. This study reports that Cp-ox/de interaction with RGD-recognizing integrins expressed on CPEpiCs affects their physiology in terms of secretome profile, proliferation inhibition, and barrier properties. This effect - promoted by the alteration of BCSFB properties - occurs under oxidative stress conditions, allowing Cp-ox/de to cross the barrier and interact with RGD-recognizing integrins expressed on the basal side of CPEpiCs. Altogether, these circumstances might contribute to neurodegeneration altering the CSF composition and worsening the BCSFB leakage already fostered by the oxidative environment.

2. Material and methods

2.1. Cell cultures and reagents

The primary human choroid plexus epithelial cells (HCPEpiCs) (ScienCell Research Laboratories) were cultured as described in (Barbariga et al., 2020). Cells were used within three culture passages to rule out de-differentiation to mesenchymal cells (Redzic, 2013). The Z310 rat choroid plexus epithelial cell line (Zheng and Zhao, 2002) was cultured as described in (Monnot and Zheng, 2013). If not specified, the chemical reagents used were from Sigma. Human plasma purified Cp was from Molecular Innovations. A synthetic peptide corresponding to the fifth type I repeat of human fibronectin (FN-I_5), containing an NGR motif, was diluted in 100 mM ammonium bicarbonate buffer, pH 8.5, and incubated for 16 h at 37 °C (FN-I_5/37 °C) in order to favour *iso*DGR motif formation (Curnis et al., 2006). Human recombinant vitronectin was from Life Technologies (cat. A14700). The antibodies used were: anti-mouse/rat α5β1 (hamster HMα5–1, Biolegend #103902) and anti-rat αVβ5 (mouse KN52, ThermoFisher #14–0497-82) for Z310 cells; anti-human α5β1 (mouse P1D6, MAB-14049, Immunological Sciences) and anti-human αVβ3 (mouse MAB-10055 clone LM609, Immunological Sciences) for HCPEpiCs cells. Control isotype monoclonal antibodies used were: Armenian Hamster IgG Isotype Control (ThermoFisher, #14–4888-81) and Mouse IgG1 κ Isotype Control (BD Pharmingen™, 550,878).

2.2. Ceruloplasmin oxidation and aging treatments

Accelerated aging and oxidation of purified Cp were carried out as described previously (Barbariga et al., 2020, 2014). Briefly, Cp was incubated (16 h at 37 °C) in 100 mM ammonium bicarbonate buffer, pH 8.5, containing 10 mM H_2O_2, *i.e.* a buffer known to favour the deamidation of the asparagine at the NGR sites and the oxidation of Cp (Barbariga et al., 2014; Olivieri et al., 2011). Bovine serum albumin (BSA) was treated in parallel as negative control. The oxidized/deamidated products were dialyzed against PBS and used fresh; they are referred in the text as oxidized/deamidated-Cp (Cp-ox/de) and oxidized/deamidated-BSA (BSA-ox/de), respectively.

2.3. Cell proliferation and apoptosis assays

Z310 cells were cultured (37 °C, 5% CO_2) in 96-well plates (10,000 cells/well) in medium containing 0.1% fetal bovine serum for a 24 h starvation. The cells were incubated for additional different times (24, 48, 72, 96, 120 h), depending on the type of assay, in the presence of Cp, Cp-ox/de, or BSA-ox/de (2–20 μg/ml). In selected experiments, cells were incubated 24 h in the presence of various concentrations of H_2O_2 (range 0–100 μM) in RPMI medium. At the end of the incubation time, cell proliferation/viability was determined by adding 3-(4,5-dimethylthiazol-2-yl)-2,5-diphenyltetrazolium bromide (MTT) solution (final concentration 0.25 mg/ml) to each well. After 2 h of incubation at 37 °C, the cell medium was removed and the formazan crystals were dissolved with dimethyl sulfoxide (200 μl/well). Absorbance was then measured at 570 nm using iMark microplate reader (BioRad). The cell number in treated wells was quantified using an external standard curve prepared by plating various amounts of Z310 cells (range 0–10^5 cell/well, in quadruplicate, 12 serial dilutions 1:2) in a 96-well plate on the day of the assay and stained in parallel with MTT. The cell viability data are reported as the percentage of seeded cells. The effect of the treatments on Z310 cell apoptosis was evaluated using annexin-V-FITC staining (Immunological Sciences), followed by flow cytometry analysis (Accuri C6 instrument, BD Biosciences and FCS Express 6 Flow v6.06.0033, DeNovo Software).

2.4. Cell adhesion assay and PIMT treatment

96-well polyvinyl chloride microtiter plates were coated with Cp or Cp-ox/de (2, 5, 20 μg/ml in PBS, 16 h at 4 °C). After washing and blocking (3% BSA in PBS), the plates were seeded with Z310 cells (40,000 cells/well in DMEM containing 0.1% BSA) and cells left to adhere 3 h at 37 °C, 5% CO_2; unbound cells were removed by washing. Adherent cells were fixed, stained with crystal violet, and quantified by measuring absorbance at 570 nm using a microplate reader (Barbariga et al., 2014). The effect of L-isoaspartyl methyltransferase (PIMT) treatment on cell adhesion was evaluated as follows: coated plates (prepared as described above) were washed and incubated with 50 μl of PIMT enzyme solution (0.02 mM S-adenosyl-L-methionine, in 50 mM Na_3PO_4, pH 6.8) supplemented with 5 μl of PIMT enzyme (IsoQuant Isoaspartate Detection kit, Promega) at 37 °C for 16 h. Then, plates were washed and the cell adhesion assays were performed as described above. In selected experiments, an *iso*DGR containing peptide (acetyl-C*iso*DGRCGVRSSSRTPSDKY, called *iso*DGR-peptide) was included as a positive control (Barbariga et al., 2015).

Competitive cell adhesions assays were performed as described above using mixtures of Z310 or HCPEpiCs cells incubated with various

amounts of Cp-ox/de or Cp (0, 3, 30, and 100 μg/ml) and seeded onto microtiter plates coated with FN-I_5/37 °C (10 μg/ml), VN (5 μg/ml), anti-integrins antibodies or isotype control monoclonal antibodies (mAb) (3 μg/ml).

2.5. Western blot analysis

Z310 cells were resuspended in lysis buffer (50 mM Tris, 150 mM NaCl, 1 mM EDTA, 1% Triton-X, 0.1% SDS, protease inhibitors cocktail, and 25 mM NaF and 5 mM $NaVO_3$ as phosphatase inhibitors). Following centrifugation (15 min, 13,000 rpm at 4 °C), the concentration of extracted proteins was quantified with Bradford assay (Bio-Rad). Proteins were resolved by 10%-acrylamide SDS-PAGE, transferred to nitrocellulose filters and analyzed by Western blot (WB) using the following antibodies: anti-ceruloplasmin (ab8813, Abcam); anti-FAK (#3285), anti-p-Tyr^{397}FAK (#3283), anti-ERK1/2 (#9102), anti-p-Thr^{202}/Tyr^{204}ERK1/2 (#9101), anti-GSK3β (#9315), anti-p-Ser^{9}GSK3β (#9336), anti-AKT (#4691), anti-p-Ser^{473}AKT (#193H12) from Cell Signaling Technology; anti-β-tubulin (T6199, Sigma.). The binding of primary antibody was detected using appropriate HRP-conjugated secondary antibodies, followed by enhanced chemiluminescence reaction (ECL reagent, GE-Healthcare) and film exposure. Films with different exposure times (5 s, 20 s, 1 min, 3 min, 10 min) were acquired by G-Box CCD-camera system (Syngene) and densitometric analysis was performed using ImageJ software (Rasband, W.S., ImageJ, U.S. National Institutes of Health, Bethesda, MD, USA). Signals were normalized to total protein loaded (Romero-Calvo et al., 2010) or to tubulin expression.

Evaluation of expression and phosphorylation of ERK1/2 was performed by Simple Western capillary immunoassay on JESS system (ProteinSimple) using the Size Separation 12–230 kDa kit. Z310 cell lysates, prepared as described above at the end of the different treatments, were transferred to the assay plate, and size-based protein separation and detection in capillaries were performed by chemiluminescence, according to the manufacturer's instruction. The antibodies used were anti-ERK1/2 (#9102) and anti-p-Thr^{202}/Tyr^{204}-ERK1/2 (#9101) from Cell Signaling Technology. Protein expression levels and phosphorylation were quantified using Compass software (ProteinSimple) and reported as p-ERK1/2:ERK1/2 signals ratio.

2.6. Secretome analysis by mass spectrometry

HCPEpiCs cells were seeded in 6-well cell culture plates (40,000 cells/well); after 24 h, the culture medium was replaced with medium without serum alone (untreated condition) or supplemented with Cp-ox/de (20 μg/ml) and the cells cultured for additionally 24 h. At the end of the incubation, the medium was recovered and centrifuged to remove cell debris; samples underwent acetone precipitation and protein concentration determined with Bradford assay. Proteins were resolved by 10%-acrylamide SDS-PAGE and stained with Coomassie blue. Each lane was cut in ten slices that were in-gel digested with trypsin (10 ng/μl, Roche) as reported (Barbariga et al., 2014). Peptides were recovered and desalted using Stage tips C18 columns (ThermoScientific), then injected in a capillary chromatographic system (EasyLC, Proxeon Biosystem). Peptides separation occurred on a homemade 25 cm long reverse-phase spraying fused silica capillary column, packed with 3-μm ReproSil 120 Å C18 AQ resin. A gradient of eluents A (2% *v*/v acetonitrile, 0.5% v/v acetic acid in water) and B (80% v/v acetonitrile, 0.5% v/v acetic acid in water) was used to achieve separation; from 10 to 35% B in 230 min, from 35 to 50% B in 5 min and from 50 to 70% B in 30 min, at 0.15 μL/min flow rate. Mass spectrometry (MS) analysis was performed using LTQ-Orbitrap mass spectrometer (ThermoScientific) equipped with nanoelectrospray ion source (Proxeon Biosystems). Full scan spectra were acquired with the lock-mass option, resolution set to 60,000, and mass range from m/z 350 to 1700 Da. The six most intense doubly and triply charged ions were selected and fragmented in the ion trap. Target ions already selected for the MS/MS were dynamically excluded for 120 s. To quantify proteins, the raw data were loaded into MaxQuant software version_1.5.2.8: label-free protein quantification was based on the intensities of precursors, both as protein intensities and normalized protein intensities (LFQ intensities). Peptides and proteins were accepted with a false discovery rate < 1%, two minimum peptides per protein with one unique. The experiments were in technical duplicates; searches were performed against the UniProt_Human Complete Proteome_cp_hum_2018_0228 with trypsin specificity, two missed cleavages allowed, cysteine carbamidomethylation as fixed modification, acetylation at protein N-terminus, and oxidation of methionine as variable modifications. Mass tolerance was set to 5 ppm and 0.6 Da, for precursor and fragment ions, respectively.

2.7. Barrier permeability analysis on cell culture transwell system

Z310 CPEpiCs barrier properties were analyzed using the cell-culture transwell system (0.4-μm pore, Transwell Support, Corning Life Sciences) pre-coated with 0.01% collagen-type 1. Cells were seeded in the upper chamber (5000 cells/well) and incubated 72 h, in the presence of 1 μM dexamethasone, until cell monolayer formation (Monnot and Zheng, 2013). Then, the cells were further incubated 24 h in the presence of different concentrations of H_2O_2 in RPMI medium (range 0–100 μM) or, in selected experiments, in the presence of 20 μg/ml Cp, Cp-ox/de or BSA-ox/de. Barrier integrity was evaluated quantifying the amount of 150 kDa FITC-dextran (FD150S, Sigma, *i.e.* a molecule with a molecular weight similar to that of Cp) in the lower chamber 30 min later its addition (100 μg) to the upper chamber, by fluorimetric analysis (Victor3 plate reader, PerkinElmer). In selected experiments, the capability of Cp, seeded in the upper chamber of the transwell (20 μg/ml in 100 μl), to cross the Z310 CPEpiCs barrier upon treatment with different concentrations of H_2O_2 (0–20-50 μM) was evaluated by WB analysis using an anti-Cp antibody on acetone-precipitated medium collected in the lower chamber. Treatment with cytochalasin B (1 μg/ml), which affects actin cytoskeleton organization, was used as control for cell barrier integrity disruption.

2.8. Integrins binding and signaling by Cp-ox/de in cell culture transwell system

Integrins engagement and signaling by Cp-ox/de upon Z310 CPEpiCs barrier alteration were evaluated by WB for ERK1/2 phosphorylation as described above. Z310 cells were cultured on transwell system until monolayer formation (see above), proteins were extracted with lysis buffer from untreated cells, from cells treated 24 h with 50 μM H_2O_2, from cells treated 2 h with 20 μg/ml Cp-ox/de, or from cells that underwent the combined treatment (Cp-ox/de + H_2O_2). Competition for Cp-ox/de integrins binding was performed by adding *iso*DGR-peptide (30 μg/ml) to the cell monolayer in the transwell system 30 min before the treatment with Cp-ox/de alone or in combination with H_2O_2. The effect of PIMT treatment on *iso*DGR-mediated binding of Cp-ox/de to integrins was evaluated as follows: before the addition to the cell culture, Cp-ox/de was incubated with S-adenosyl-L-methionine and PIMT solution (as described above) and then used alone or in combination with H_2O_2 in the assay for the evaluation of integrin engagement and signaling across the Z310 CPEpiCs barrier. In selected experiments, after different treatments, the amount of Cp-ox/de bound to CPEpiCs was evaluated on protein extracts by WB performed with anti-Cp antibody.

2.9. Immunofluorescence analysis

Z310 cells were cultured on coverslip glasses (13 mm Ø x 170 μm) coated with poly-L-lysine until they formed a confluent monolayer. Cells were treated with different concentrations of H_2O_2 (0–20-50 μM) or cytochalasin B (1 μg/ml) as described above. After treatments, cells were fixed with 4% paraformaldehyde, permeabilized with 0.5% saponin and

immunostained with a mouse anti-ZO1 antibody (339,100, Invitrogen) followed by an Alexa-546-conjugated goat-anti-Mouse IgG (A11003, Invitrogen) secondary antibody. Alexa-647-conjugated phalloidin (A22287, Invitrogen) and Hoechest-33,342 (Invitrogen) were used for actin and nuclei staining, respectively. Staining was assessed by confocal microscopy (Leica TCS SP5 Laser Scanning Confocal), and images were acquired with LAS-AF software (Leica).

2.10. Statistical and bioinformatics analysis

Statistical significance among three or more groups was evaluated by One-way Analysis of Variance (ANOVA) if the data passed the normality test for Gaussian distribution (Kolmogorov-Smirnov test) or Kruskal-Wallis test. *Ad hoc* post-test analysis was performed to compare all pairs of groups or selected pairs of groups; respectively, Tukey's or Bonferroni's or Holm-Šídák's test were used for the ANOVA. The Dunn's test was used in the case of Kruskal-Wallis analysis. In selected analysis,

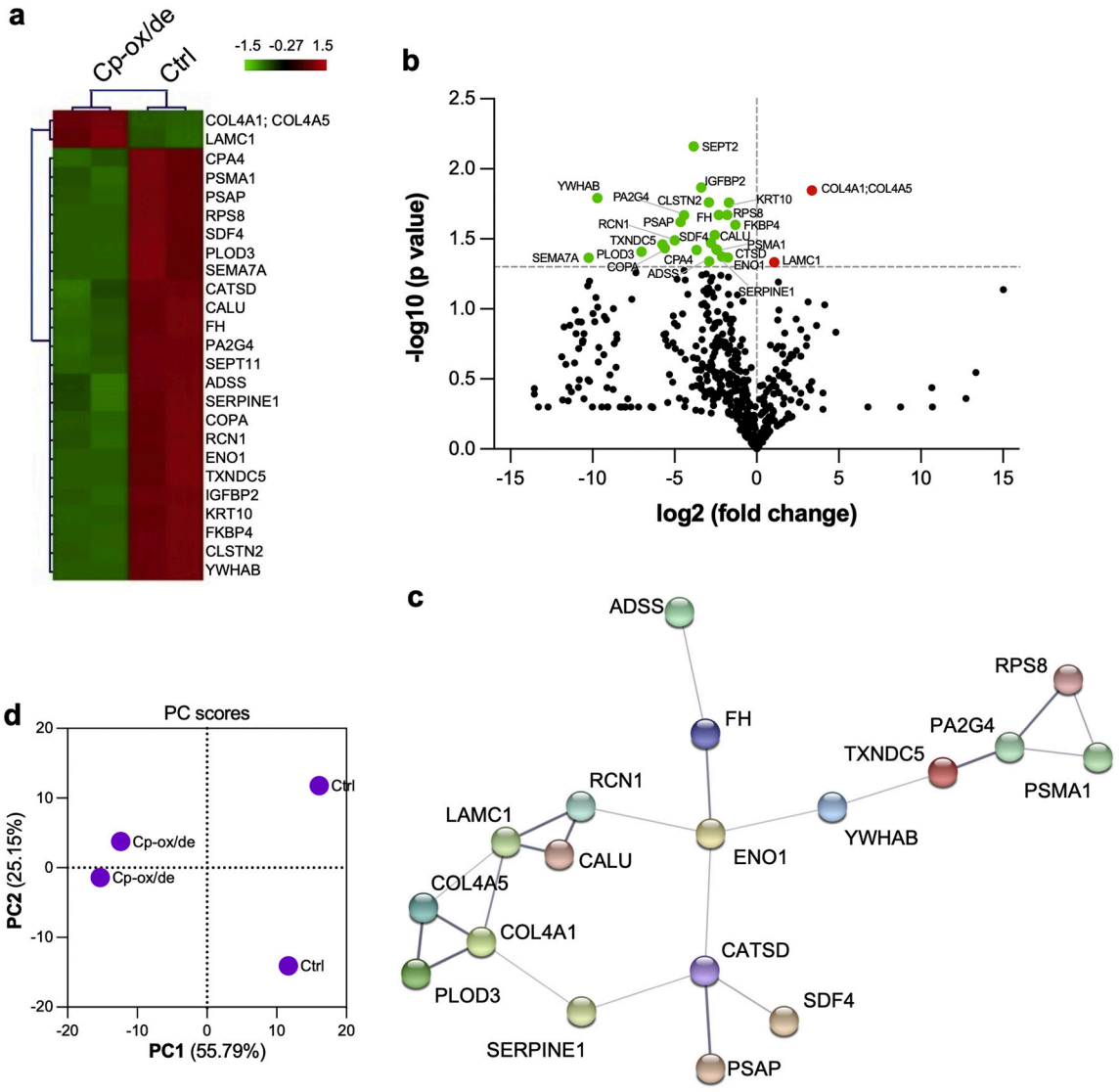

Fig. 1. Proteins showing different levels in the secretome of primary human choroid plexus epithelial cells (HCPEpiCs) treated with Cp-ox/de. a) Hierarchical cluster analysis of label free quantification intensities derived from MaxQuant elaboration of MS spectra; the heat-map shows proteins found to have different levels of secretion between untreated (Ctrl) and Cp-ox/de treated HCPEpiCs ($p < 0.05$, MeV software, student-t); up- and down-regulated proteins are indicated in red and green, respectively; [COL4A1 and A5, collagen-α1(IV) and-α5(IV); LAMC1, laminin subunit-γ1; PSMA1, proteasome subunit α type-1; PSAP, prosaposin; RPS8, 40S ribosomal protein-S8; CPA4, carboxypeptidase-A4; PLOD3, Multifunctional procollagen lysine hydroxylase and glycosyltransferase LH3; SDF4, 45 kDa calcium-binding protein; SEMA7A, semaphorin-7A; CATSD, cathepsin-D; CALU, calumenin; FH, fumarate hydratase, mitochondrial; PA2G4, proliferation-associated protein-2G4; SEPT11, septin-11; ADSS, adenylosuccinate synthetase isozyme-2; SERPINE1, plasminogen activator inhibitor-1; COPA, coatomer subunit-α; RCN1, reticulocalbin-1; ENO1, α-enolase isoform-2; TXNDC5, thioredoxin domain-containing protein-5; IGFBP2, insulin-like growth factor-binding protein-2; KRT10, keratin type-I cytoskeletal-10; FKBP4, peptidyl-prolyl cis-trans isomerase FKBP4; CLSTN2, calsyntenin-2; YWHAB, 14–3-3 protein β/α]. b) Volcano plot analysis performed on the 468 identified proteins. The y-axis shows the negative log10 *p* value (dashed line at y = 1.3 indicates a p value of 0.05) and the x-axis the log2 of the fold change of protein levels in the secretoma of Cp-ox/de-treated cells *vs.* untreated cells as evaluated by MeV software. Proteins with significant different levels of secretion in Cp-ox/de-treated cells are highlighted in red (increased levels) or green (decreased levels). c) Protein network highlighted by protein-protein interaction STRING analysis within the 25 proteins showing different levels of secretion. Connection lines: thin = interaction confidence >0.400; thick = interaction confidence >0.900. d) Multivariate unsupervised principal component analysis (PCA) performed on the 468 identified proteins; Cp-ox/de samples are distinguished from control (Ctrl) samples; analysis was assessed by Prism 9 software. (For interpretation of the references to colour in this figure legend, the reader is referred to the web version of this article.)

due to the large variability obtained in the biological replicates, the Wilcoxon matched-pairs signed rank test had been used to compare different treatments and controls within the same experiments. In all analyses, a p value <0.05 was considered statistically significant comparing means ± standard error (SEM). All the analyses were performed with Prism V9.1.1 software (GraphPad Inc.). Multi-Experiment Viewer, MeV software v4.9.0 was used for the secretome data analysis to generate unsupervised hierarchical clustering heat-map and volcano plot. Prism V9.1.1 software was used for principal component analysis (PCA). Gene Ontology (GO) -Cellular Component enrichment analysis was performed using Panther Classification System v13 (Panther Overrepresentation test) and GO database Released 2018_06_01. Protein-protein interaction network analysis and functional pathway enrichment analysis were performed using STRING v11.0 software.

3. Results

3.1. Cp-ox/de treatment affects the secretome profile of primary HCPEpiCs

Since CPEpiCs mainly determine CSF composition, we investigated the effect that integrins engagement, *via* modified-Cp, has on the secretome, namely the whole set of proteins released in the CSF by the CPEpiCs, as secreted proteins, part of microvesicles/exosomes and extracellular matrix (ECM) components. Cp-ox/de mediates cell adhesion and signal transduction in HCPEpiCs, that do express αVβ3 and α5β1 integrins suitable for *iso*DGR motif binding (Barbariga et al., 2020). In the secretome of Cp-ox/de-treated or untreated HCPEpiCs we identified and quantified by mass spectrometry analysis a total of 468 proteins (Supplemental Materials, SM: Table-SM1a). Within these proteins, the Gene Ontology (GO) Cellular Component enrichment analysis showed a significant overrepresentation of proteins belonging to the extracellular environment and the cell-cell and the cell-ECM interaction, indicating the specificity of the investigated sub-proteome (SM: Fig. SM1; Table-SM2).

Differential protein levels analysis between Cp-ox/de treated and control (Ctrl) untreated HCPEpiCs showed 25 proteins with significant different levels (as performed by MeV software *t*-test, $p < 0.05$) highlighted by hierarchical clustering and volcano plot representation (Fig. 1a and b; SM: Table-SM1b). A brief description of the features of the proteins showing different levels of secretion is provided in Supplemental Materials Text-SM1. Based on their characteristics, most of these proteins can be grouped according to their involvement in cell growth and proliferation, protease activity, protein synthesis and processing, basement membrane and ECM organization, neurons functionality, neurodegeneration, integrins functionality and barrier permeability (SM: Fig. SM2). The level of most of these proteins was downmodulated in Cp-ox/de treated cells compared to untreated cells, while 2 proteins, collagen-IV-α1/−α5 and laminin-C1 were up-regulated (Fig. 1a, b). In the case of collagen, based on the identified peptides, discrimination between the two protein isoforms α1/−α5 was not possible. Protein-protein interaction network analysis generated by STRING among the 25 proteins showing different levels of secretion highlighted a network of 18 proteins (Fig. 1c). The network showed *inter alia* the significant enrichment in pathways related ECM interaction and rearrangement (*i.e.* ECM-receptor interaction, focal adhesion, regulation of plasminogen activation, basement membrane organization, ECM organization) intracellular signaling (*i.e.* estrogen signaling, AGE-RAGE signaling, PI3K-Akt signaling, collagen-activated tyrosine kinase receptor signaling) and exocytosis (SM: Table-SM1c). These enrichments suggested the role of integrins engagement by Cp-ox/de in the modification of HCPEpiCs functionality by transducing intracellular signaling that affects cells secretome and their anchorage to the ECM. Differences in protein secretome profiles were underlined by multivariate unsupervised analysis, performed by principal component analysis (PCA) on the 468 identified proteins. Limitations of our study were the restricted number of replicates we analyzed and the use of label-free method for protein quantitation. The first was due to the use of primary HCPEpiCs cells that cannot be cultured for a long time without serum and cannot be expanded sufficiently because they de-differentiate to fibroblast; the second because resulted in data variability, in particular in the control group. Nevertheless, the PCA was able to clearly distinguish Cp-ox/de samples from control (Ctrl), and the two groups were mainly separated in PC1, which explains >55% of the variance within the dataset (Fig.1d).

3.2. Cp-ox/de inhibits the adhesion of primary HCPEpiCs mediated by α5β1 and αVβ3 integrin

To demonstrate that Cp-ox/de could bind the RGD-binding integrins αVβ3 and α5β1 expressed by the HCPEpiCs (Barbariga et al., 2020) we analyzed the effect of Cp-ox/de on HCPEpiCs adhesion mediated by coated-plate with anti-α5β1 mAb P1D6 and anti-αVβ3 mAb LM609, *i.e.* two functional antibodies capable to promote cell adhesion. The results showed that Cp-ox/de, but not unmodified Cp, was able to inhibit the HCPEpiCs adhesion in dose-dependent fashion (α5β1: ANOVA, $p < 0.0001$; Holm-Šídák's post-test $p < 0.0001$ and $p = 0.0163$ for Cp-ox/de at 100 μg/m and at 30 μg/ml, respectively. αVβ3: ANOVA, $p < 0.0001$; Holm-Šídák's post-test $p < 0.0001$ and $p = 0.0059$ for Cp-ox/de at 100 μg/m and at 30 μg/ml, respectively) (Fig. 2a and b). Since it is known that the epitope recognized by the LM609 mAb is located very closely to the RGD-binding site in αVβ3 integrin (Borst et al., 2017), the Cp-ox/de-mediated inhibition of cell adhesion to this mAb was likely due to steric hindrance between the two molecules. Differently, P1D6 mAb does not inhibit α5β1 integrin interactions with the RGD site in fibronectin but inhibits α5β1 interactions with the synergy site of fibronectin (Mould et al., 1997). Therefore, inhibition of the interaction of α5β1 with P1D6 mAb, mediated by the Cp-ox/de, might be caused by an indirect competition of the interactions of the mAb with the epitope on α5β1 integrin, due to steric hindrance between large molecules, or, in alternative, the binding of Cp-ox/de might induce a conformational change of the α5β1 integrin that prevents further interactions dependent on the epitope recognizing the synergy site on fibronectin.

Together, these results clearly demonstrated that Cp-ox/de directly binds, at least, α5β1 and αVβ3 RGD-binding integrins on HCPEpiCs

3.3. Cp-ox/de inhibits the adhesion of primary HCPEpiCs mediated by deamidated fifth type I repeat of fibronectin and vitronectin

Next, we investigated whether Cp-ox/de, binding to the RGD-recognizing integrins, could affect the HCPEpiCs adhesion to ECM proteins, such as the deamidated fifth type I repeat of fibronectin (FN-I_5/37 °C) and vitronectin (VN). FN-I_5/37 °C was chosen because it contains an NGR motif which, upon forced deamidation, generates an *iso*DGR motif that specifically binds the αVβ3 integrin and promotes αVβ3-mediated cell adhesion (Curnis et al., 2006). The results showed that Cp-ox/de inhibited in a dose-dependent manner the cell adhesion and spreading on both VN- and FN-I_5/37 °C-coated plates (VN: ANOVA, $p < 0.0001$; Holm-Šídák's post-test $p < 0.0001$ and $p = 0.0043$ for Cp-ox/de at 100 μg/m and at 30 μg/ml, respectively. FN-I_5/37 °C: ANOVA, $p < 0.0001$; Holm-Šídák's post-test $p < 0.0001$ and $p = 0.0016$ for Cp-ox/de at 100 μg/ml and at 30 μg/ml, respectively) (Fig. 2c and d). Notably, the highest concentration of unmodified Cp caused a slight inhibition of cell adhesion to VN-coated plates, but not to FN-I_5/37 °C-coated plates (Holm-Šídák's post-test $p = 0.0432$). This modest effect might be due to the spontaneous deamidation of Cp, which can occur during purification procedures and storage. These results demonstrated that Cp-ox/de can act as antagonist of RGD-containing ligands (or *iso*DGR-containing ligands) of the ECM and preventing the binding to RGD-recognizing integrins.

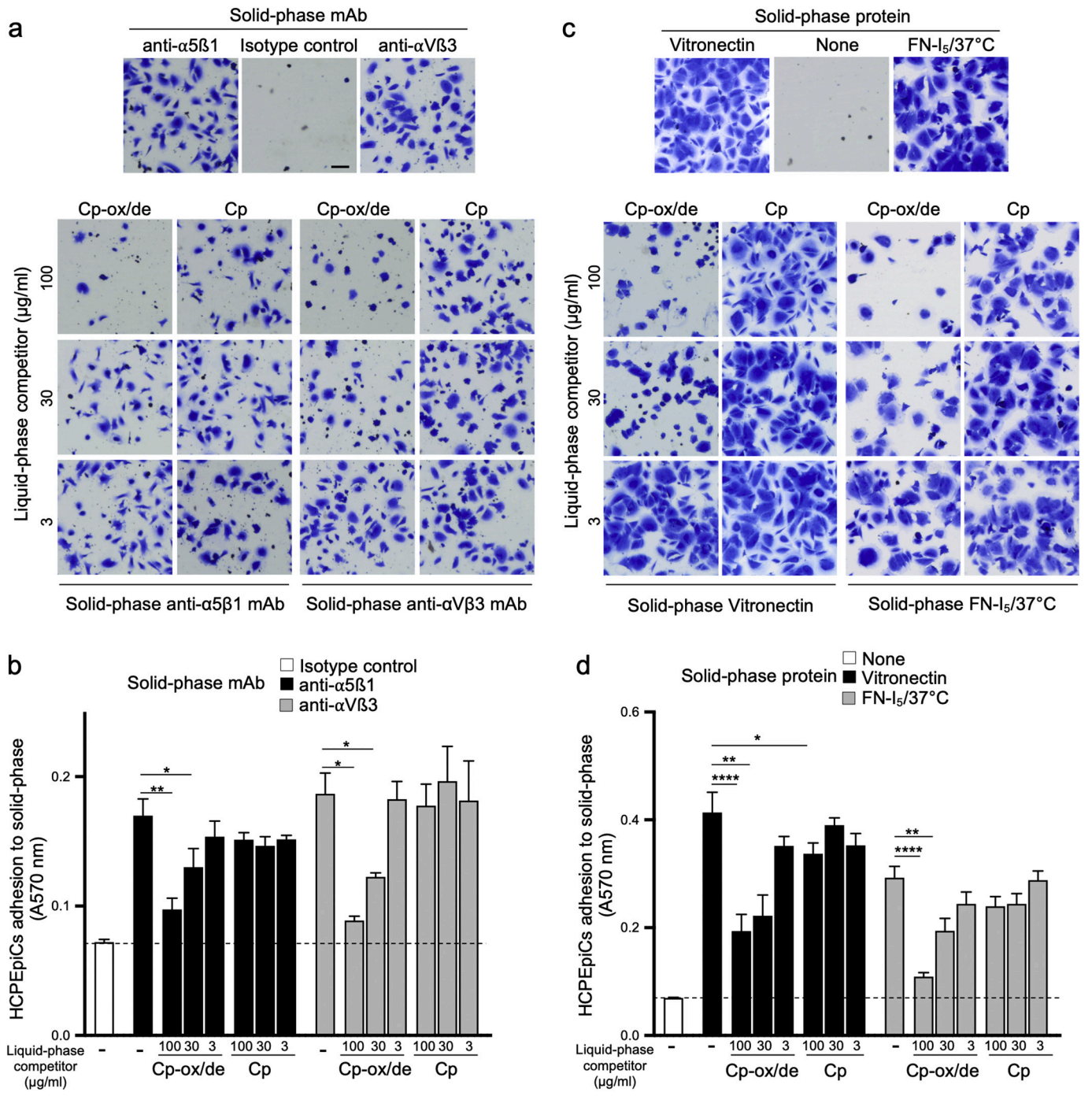

Fig. 2. Cp-ox/de inhibits HCPEpiCs adhesion mediated by anti-α5β1 and anti-αVβ3 antibodies, vitronectin and deamidated fifth type I repeat module of human fibronectin (FN-I_5/37 °C). a and c, upper panels) Adhesion of HCPEpiCs to microtiter plates coated with the indicated anti-integrin antibodies, isotype control antibodies and ECM proteins. Representative microphotographs of adherent cells to wells coated with the indicated antibodies and proteins are shown. a and c, lower panels) Effect of various doses of Cp-ox/de and unmodified Cp (*Liquid-phase competitor*) to cells adhesion to plates coated with the indicated antibodies and proteins (*Solid-phase*). Representative microphotographs of the effect of Cp-ox/de and unmodified Cp on cell adhesion are shown. b and d) Cell adhesion quantification by crystal violet staining of experiments depicted in panels a and c). Cell adhesion assays were carried out as described in "Materials and Methods" using 15,000 cells/well. Statistical significance p value in panel b and d was evaluated by One-way ANOVA ($p < 0.0001$) comparing means ± SEM ($n = 3$ with 3 replicates each) with Holm-Šídák's post-test (*, $p < 0.05$; **, $p < 0.01$; ****, $p < 0.0001$). Dashed line indicates the background level. Scale bar = 100 µm. (For interpretation of the references to colour in this figure legend, the reader is referred to the web version of this article.)

3.4. Cp-ox/de mediates Z310 choroid plexus epithelial cells adhesion via isoDGR/integrin binding, interacts with α5β1 and αVβ5 integrins and competes for cell adhesion to vitronectin

Primary HCPEpiCs have been reported not suitable for barrier studies due to the lack of tight junctions formation in culture (Redzic, 2013). To study the effect of Cp-ox/de on BCSFB properties, we used the Z310 murine CPEpiC line, which has been described to be appropriate for barrier permeability studies (Zheng and Zhao, 2002). Flow cytometry and WB analysis showed that Z310 cells do express αVβ5 and α5β1 integrins suitable for *iso*DGR motif binding (Barbariga et al., 2014; Corti and Curnis, 2011), but not the αVβ3, αVβ6 and αVβ8 heterodimers

(Fig. SM3).

Similarly to what reported for HCPEpiCs (Barbariga et al., 2020), Z310 cells showed dose-dependent adhesion to plates coated with Cp-ox/de, but not to plates coated with untreated Cp (ANOVA, $p < 0.0001$; Tukey's post-test Cp *vs.* Cp-ox/de $p < 0.01$ at 5 μg/ml; $p < 0.001$ at 20 μg/ml) (Fig. 3a). Pre-treatment of the plates coated with Cp-ox/de or coated with a control *iso*DGR-peptide with PIMT, an enzyme that converts *iso*Asp to Asp (Curnis et al., 2006), inhibited their pro-adhesive activity (ANOVA, $p < 0.0001$; Bonferroni's post-test $p < 0.0001$ for Cp *vs.* Cp-ox/de and Cp *vs. iso*DGR, $p < 0.001$ for *iso*DGR *vs. iso*DGR + PIMT, $p < 0.05$ for Cp-ox/de *vs.* Cp-ox/de + PIMT) (Fig. 3b and c). This pointed out that cell adhesion to Cp-ox/de was mediated by the *iso*DGR motifs, since the DGR motif is not structurally suitable for integrin binding (Curnis et al., 2006). Differently from HaCaT (Barbariga et al., 2014) and HCPEpiCs, Z310 cells showed limited cell spreading on both Cp-ox/de and *iso*DGR-peptide (Fig. 3c).

Analogously to what was observed for HCPEpiCs, but in accord with the integrins expressed by the Z310 cells, Cp-ox/de inhibited the Z310 cell adhesion to microtiter plates coated with anti-α5β1 mAb HMα5–1, anti-αVβ5 mAb KN52 (*i.e.*, two functional antibodies capable to promote cell adhesion) and vitronectin (α5β1: Kruskal-Wallis test, p < 0.0001; Dunn's post-test $p = 0.0010$ and $p = 0.0337$ for Cp-ox/de at 100 μg/m and at 30 μg/ml, respectively; αVβ5: Kruskal-Wallis test, p < 0.0001; Dunn's post-test $p = 0.0203$ and $p = 0.0104$ for Cp-ox/de at 100 μg/ml and at 30 μg/ml, respectively; VN: ANOVA, p < 0.0001; Holm-Šídák's post-test p < 0.0001 for Cp-ox/de both at 100 μg/m and at 30 μg/ml) (Fig. 4a, b, c and d). These effects were not seen using for the competition the unmodified Cp. As expected, Z310 cells did not adhere to wells coated with deamidated FN-I_5, confirming the lack of αVβ3 integrin expression (Fig. 4c and Fig. SM3). Together these results demonstrated that Cp-ox/de directly binds α5β1 and αVβ5 integrins expressed on Z310 cells and confirm that Cp-ox/de can act as antagonist of RGD-containing ligands (or *iso*DGR-containing ligands) of the ECM for the binding to RGD-recognizing integrins.

3.5. *Cp-ox/de binding to Z310 CPEpiCs transduces an intracellular signal and results in proliferation inhibition*

In Z310 cells, the binding of Cp-ox/de to integrins was able to trigger intracellular signaling underlined by the phosphorylation of the activation residues Thr^{202}/Tyr^{204} of ERK1/2 (Fig. 5a). Contrary to what was observed for HCPEpiCs, neither FAK nor GSK3β molecules were found to

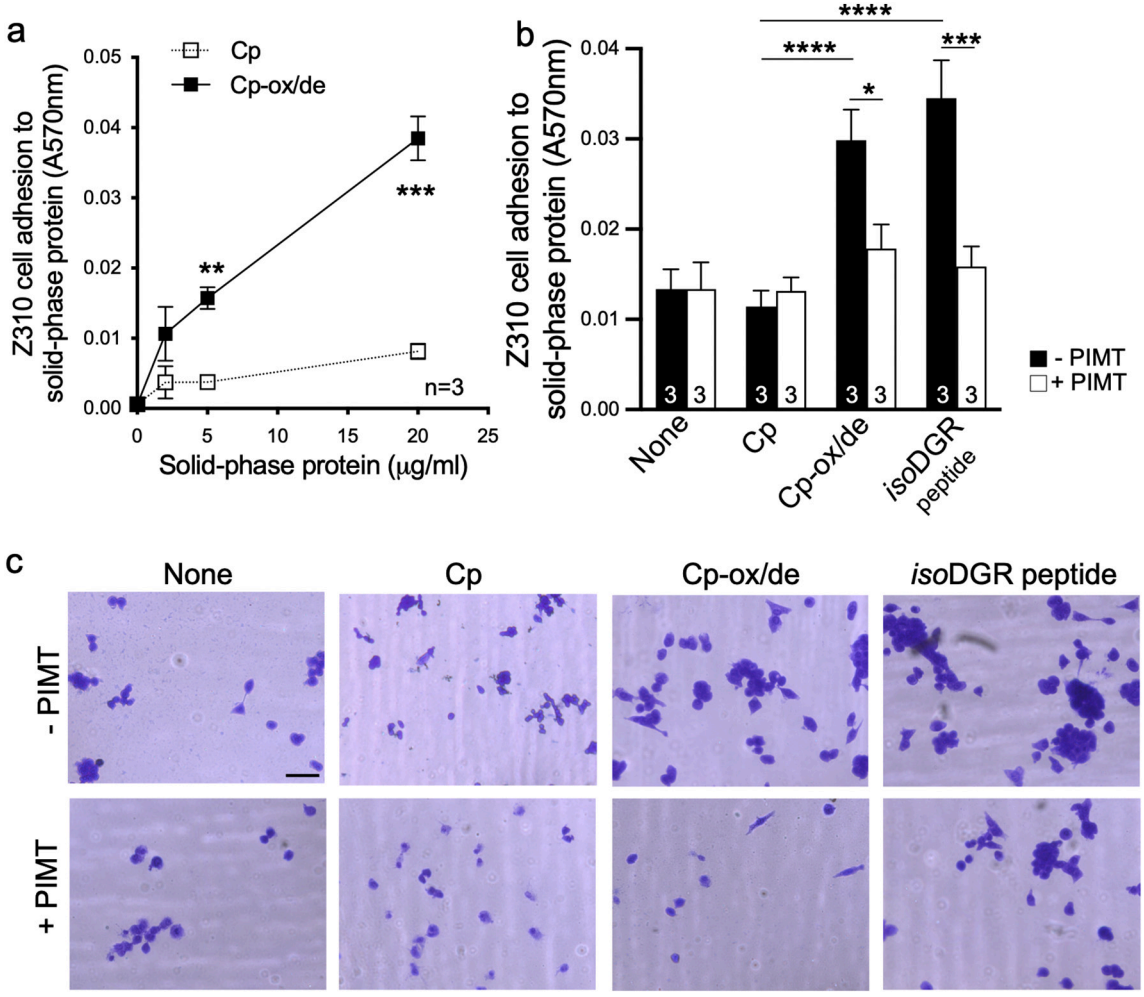

Fig. 3. Cp deamidation mediates Z310 cell adhesion *via iso*DGR-integrins interaction. a) Adhesion of Z310 cells to plates coated with different amount of either Cp or oxidized/deamidated-Cp (Cp-ox/de). Adhesion was evaluated as absorbance at 570 nm of the crystal violet stained cells. ANOVA, $p < 0.0001$. b) Inhibition of Z310 cells adhesion occurs after treatment of Cp-ox/de and Cp coating proteins (20 μg/ml) with PIMT (+) compared to the untreated wells (−). Coating with *iso*DGR-peptide (20 μg/ml) was used as positive control. c) Representative images of stained cells adherent to Cp or Cp-ox/de or *iso*DGR peptide coating treated with (+) or without (−) PIMT enzyme are shown. Scale bar = 50 μm. ANOVA, p < 0.0001; post-test **** for Cp *vs.* Cp-ox/de and Cp *vs. iso*DGR, *** for *iso*DGR *vs. iso*DGR + PIMT, * for Cp-ox/de *vs.* Cp-ox/de + PIMT. Statistical significance p value was evaluated by One-way ANOVA comparing means ± SEM (n = 3 with 3 replicates each) with Tukey's post-test analysis in panel a or Bonferroni's post-test analysis in panel b (*, p < 0.05; **, p < 0.01; ***, $p < 0.001$; ****, p < 0.0001). (For interpretation of the references to colour in this figure legend, the reader is referred to the web version of this article.)

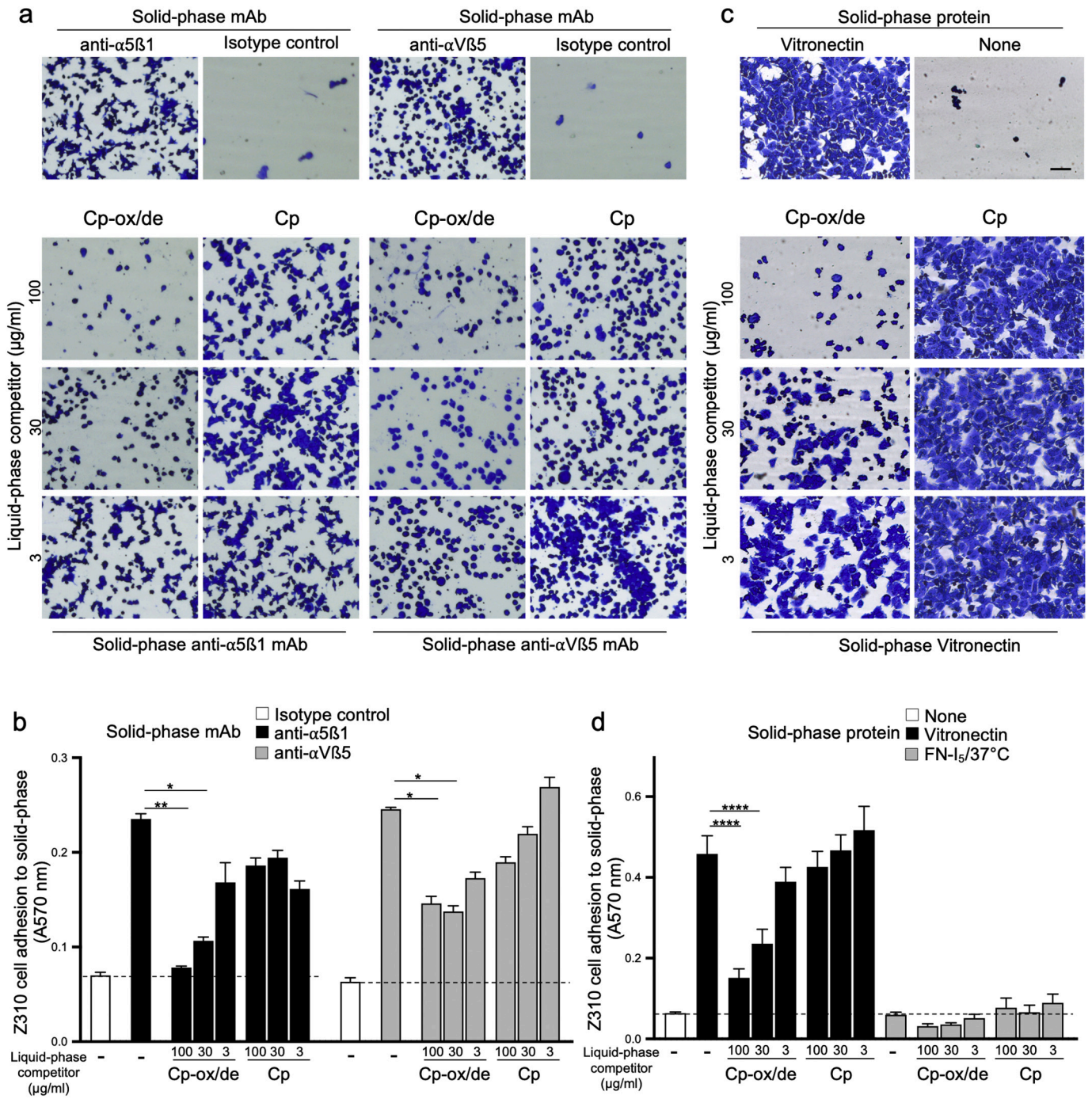

Fig. 4. Cp-ox/de inhibits Z310 cell adhesion mediated by anti-α5β1 and anti-αVβ5 antibodies and vitronectin. a and c, upper panels) Adhesion of Z310 to microtiter plates coated with the indicated anti-integrin antibodies, isotype control antibodies and proteins. Representative microphotographs of adhered cells to wells coated with the indicated antibodies and vitronectin are shown. a and c, lower panels) Effect of various doses of Cp-ox/de and unmodified Cp (*Liquid-phase competitor*) to cells adhesion to plates coated with the indicated antibodies and vitronectin (*Solid-phase*). Representative microphotographs of the effect of Cp-ox/de and unmodified Cp on cell adhesion are shown. Note that no cells adhesion to FN-I_5/37 °C coated wells was observed. b and d) Cell adhesion quantification by crystal violet staining of experiments depicted in panels a and c). Cell adhesion assays were carried out as described in "Material and Methods" using 40,000 cells/well. Statistical significance p value comparing means ± SEM (n = 3 with 3 replicates each) was evaluated in panel b by Kruskal-Wallis test ($p < 0.0001$) with Dunn's post-test, and in panel d by One-way ANOVA ($p < 0.0001$) with Holm-Šídák's post-test (*, $p < 0.05$; **, $p < 0.01$; ****, $p < 0.0001$). Dashed line indicates the background level. Scale bar = 50 µm. (For interpretation of the references to colour in this figure legend, the reader is referred to the web version of this article.)

be phosphorylated (Fig. 5a). Z310 cells showed proliferation reduction after 48 h and 96 h of incubation with Cp-ox/de (ANOVA, $p < 0.0001$; Bonferroni's post-test $p < 0.05$ for Cp *vs.* Cp-ox/de at 48 h and $p < 0.001$ at 96 h, $p < 0.01$ for Cp-ox/de *vs.* BSA-ox/de at 96 h), while treatment with either unmodified Cp or BSA-ox/de were uneffective in inhibiting Z310 cell proliferation (Fig. 5b). Therefore, similarly to HCPEpiCs cells (Barbariga et al., 2020), Cp-ox/de interacts with Z310 murine CPEpiCs throughout integrins binding, mediated by *iso*DGR motifs, which in turn transduces an intracellular signal which results in cells proliferation inhibition. Contrary to the epidermal epithelial HaCaT cells (38), the signal transduced in Z310 cells did not promote cell apoptosis, as assessed by annexin-V staining after 72 h and 96 h treatment with Cp-

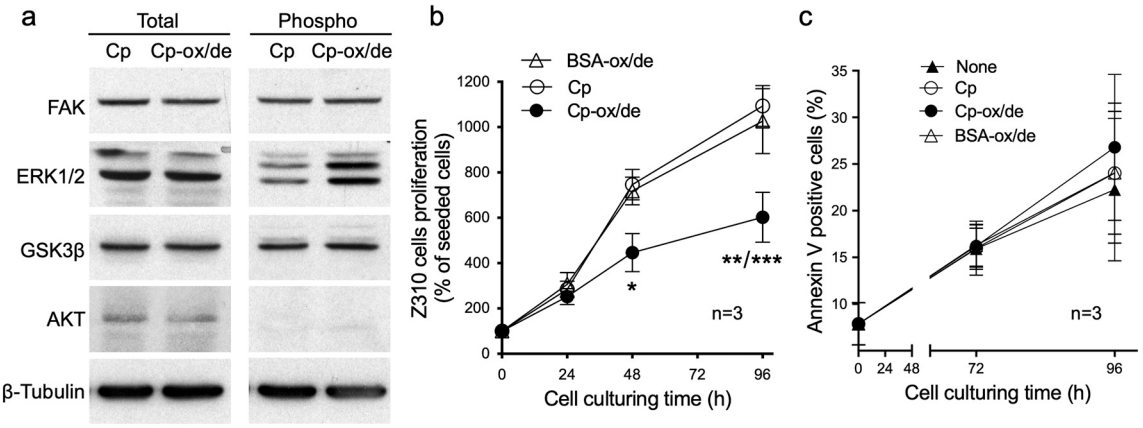

Fig. 5. *Via iso*DGR-integrins interaction Cp-ox/de transduces an intracellular signal promoting Z310 cell proliferation inhibition. a) Western blot analysis of the signal transduced by Cp-ox/de in Z310 cells treated (2 h, 5 μg/ml) with either Cp or Cp-ox/de. Total protein expression (Total) and phosphorylation of specific residues (Phospho) was evaluated in the cell lysate for FAK and p-Tyr^{397}FAK, ERK1/2 and p-Thr$^{202/}$Tyr^{204}ERK1/2, GSK3β and p-Ser^{9}GSK3β, AKT and p-Ser^{473}AKT. Signals were normalized by β-Tubulin. Cropped images are from the same or twin SDS-PAGE, with different film exposure to avoid signal saturation. b) Proliferation measured by MTT assay on Z310 cells. Cells were incubated for different times with 5 μg/ml of untreated Cp, Cp-ox/de or BSA-ox/de. Cells number was reported as percentages of the seeded cells. Statistical p value was evaluated by One-way ANOVA comparing means ± SEM (n = 3 with 6 replicates each) with Bonferroni's post-test analysis (ANOVA, $p < 0.0001$; post-test for Cp *vs.* Cp-ox/de * at 48 h and *** at 96 h, for Cp-ox/de *vs.* BSA-ox/de ** at 96 h) (*, $p < 0.05$; **, $p < 0.01$; ***, $p < 0.001$; ****, $p < 0.0001$). c) Apoptosis detection. Z310 cells were incubated for 72 and 96 h as they are (None) or with 5 μg/ml of untreated Cp, Cp-ox/de or BSA-ox/de; cells were then stained with annexin-V FITC and analyzed by flow cytometry. Percentage of annexin-V positive cells at different times is reported as means ± SEM (n = 3). See Supplemental Materials Figure SM4 for gating strategy and flow cytometry profiles of a representative experiment.

ox/de (Fig. 5c; SM4). In the medium of the Z310 cells treated with Cp-ox/de we validated by WB the levels of some of the proteins showing different levels in the secretome of HCPEpiCs; we found an increase of Laminin C1 and a decrease of α-enolase, SERPIN 1, prosaposin and cathepsin D (Fig SM5).

3.6. Oxidative environment induces choroid plexus epithelial cell barrier leakage, which allows Cp to cross the barrier

Integrins are usually expressed on the basal side of epithelial monolayers (Lee and Streuli, 2014). Therefore, on CPEpiCs that face the CSF by the apical side, integrins engagement by modified-Cp is likely unfeasible due to the presence of tight junctions, unless the oxidative conditions found in the PD-CSF affects the BCSFB properties (Barbariga et al., 2015). Confocal microscopy analysis confirmed the basal expression of integrins in a sealed monolayer of Z310 cells, showing β5- and β1-integrin expression in basal sections of z-axes compared to the expression of the tight junction marker ZO1 found in more apical sections (Fig. SM6A and B).

The cell culture transwell system was used to investigate the barrier permeability properties of the Z310 CPEpiCs monolayer. Treatments either with Cp, Cp-ox/de or BSA-ox/de were *per se* not able to affect the barrier properties of the Z310 CPEpiCs, while cytochalasin B, *i.e.* a well-known agent capable to disgregate actin-cytoskeleton organization necessary to maintain barrier function, as expected induced barrier disruption (Fig. 6a). CPEpiCs treatment with increasing concentration of H_2O_2 showed that a barrier leakage was induced at a concentration of 50 μM (ANOVA, $p < 0.0005$; Tukey's post-test $p < 0.01$ for 0 *vs.* 50 μM H_2O_2 and 20 *vs.* 50 μM H_2O_2, $p < 0.05$ for 10 *vs.* 50 μM H_2O_2, 30 *vs.* 50 μM H_2O_2 and 40 *vs.* 50 μM H_2O_2) (Fig. 6b). This concentration is similar to that found in the CSF of PD patients (Barbariga et al., 2015). The outflow of dextran-FITC, used as a reporter of barrier leakage, induced by 50 μM H_2O_2 was about 20% of that observed when the complete barrier disruption was induced by cytochalasin B treatment (Fig. 6b). Interestingly, this treatment caused also the passage of Cp across the cell barrier (ANOVA, $p = 0.0028$; Tukey's post-test $p < 0.01$ for 0 *vs.* 50 μM H_2O_2, $p < 0.05$ for 20 *vs.* 50 μM H_2O_2), with a Cp outflow of about 40% of that one induced by cytochalasin B treatment (Fig. 6c and d). This effect was not due to cells death because Z310 cells viability was not affected by incubation with 50 μM H_2O_2, at least at 24 h, even though cell proliferation was reduced (Fig. SM7). Differences in cell number might also contribute to the observed reduced barrier properties; however, since in the transwell experiments cells were treated with H_2O_2 when they already had reached the monolayer confluence status, it is unlikely that the proliferation slow down would have affected the barrier properties.

3.7. Oxidative environment promotes tight junctions disassembly and actin cytoskeleton rearrangement in choroid plexus epithelial cell

Confocal microscopy analysis on Z310 monolayer indicated that the barrier leakage induced by treatment with H_2O_2 concentrations similar to those found in the CSF of PD patients, might be due to actin cytoskeleton re-organization and tight junctions disassembly. Indeed, while treatment with 20 μM H_2O_2 did not alter/modify the continuous staining on the cell edges of the tight junction marker ZO1, the staining was rearranged in discontinuous dots upon treatment with 50 μM H_2O_2 (Fig. 7). In cells treated with 50 μM H_2O_2, a disorganizing effect was also observed on the actin cytoskeleton (Fig. 8). Actin lost its organization on cell edges aimed to give rigidity to a sealed epithelial barrier in favour of a dispersed irregular filamentous staining (Fig. 8). Thus, the actin cytoskeleton rearrangement and the tight junctions disassembly might promote barrier leakage. Nevertheless, 50 μM H_2O_2 concentration treatment did not induce a complete destructuring of the cell monolayer, as it occurred when cells were treated with cytochalasin B, which induced cells retraction and generation of evident holes in the monolayer (Fig. SM8). These results suggested that pathological oxidative conditions may induce BCSFB leakage that allows Cp to cross the barrier.

3.8. Cp-ox/de crosses the choroid plexus epithelial cell barrier under oxidative conditions and transduces an intracellular signal via integrin binding

Using the Z310 CPEpiCs monolayer model, we next investigated whether, under oxidative conditions, the Cp-ox/de that crossed the barrier was able to engage integrins. We found that the RGD-recognizing integrin profile was not changed upon H_2O_2 treatment in Z310 (Fig. SM3D). The combined treatment of 50 μM plus Cp-ox/de was able

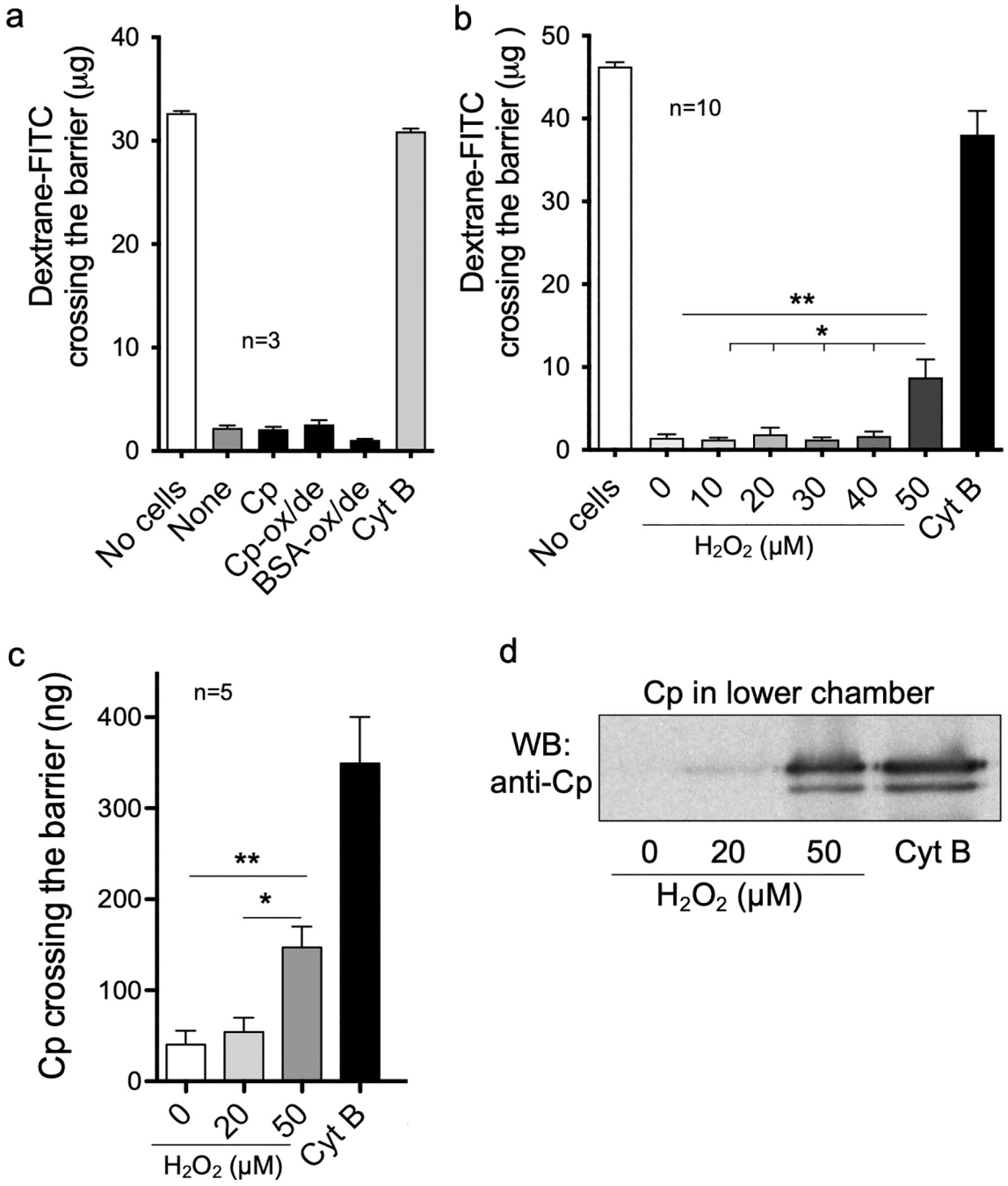

Fig. 6. Oxidative environment promotes choroid plexus epithelial cell barrier leakage. a) Z310 cell cultures on transwell-system were treated 24 h with 20 μg/ml of either Cp, Cp-ox/de, BSA-ox/de or 2 h with cytochalasin B (Cyt B) (1 μg/ml). Barrier permeability was measured evaluating the amount of dextran-FITC, dispensed in the upper chamber (100 μg), that was recovered in the bottom chamber (n = 3 with 3 replicates each). b) Barrier permeability was measured as in panel A, but cells were treated 24 h with increasing concentration of H_2O_2 or Cyt B as control. Statistical significance p value was evaluated by One-way ANOVA ($p = 0.0005$) comparing means ± SEM ($n = 10$) with Tukey's post-test analysis (*, $p < 0.05$; **, $p < 0.01$; ***, $p < 0.001$; ****, $p < 0.0001$). c) Barrier permeability was measured as in panel A by evaluating the amount of Cp that crosses the cell monolayer; cells were treated 24 h with either 0, 20, or 50 μM H_2O_2 or 2 h with Cyt B as control. Cp (2 μg) was administered into the upper chamber and the amount that crossed the barrier after 1 h incubation was evaluated by WB analysis on the acetone-precipitated medium recovered from the bottom chamber. Statistical significance p value was evaluated by One-way ANOVA ($p = 0.0028$) comparing means ± SEM ($n = 5$) with Tukey's post-test analysis (*, $p < 0.05$; **, $p < 0.01$; ***, $p < 0.001$; ****, $p < 0.0001$). d) A representative WB of Cp signal found in the transwell bottom chamber at the end of the incubation.

to foster ERK1/2 phosphorylation (ANOVA, $p < 0.0001$; Bonferroni's post-test $p < 0.01$ for untreated *vs.* H_2O_2 + Cp-ox/de, $p < 0.05$ for H_2O_2 *vs.* H_2O_2 + Cp-ox/de, $p < 0.05$ for Cp-ox/de *vs.* H_2O_2 + Cp-ox/de), while treatment with either H_2O_2 or Cp-ox/de alone were not (Fig. 9). The hypothesis that signal transduction was mediated by Cp-ox/de binding to RGD-recognizing integrins was supported by the evidence that ERK1/2 phosphorylation induced by H_2O_2 + Cp-ox/de treatment was inhibited by both competition with *iso*DGR-peptide and Cp-ox/de pretreatment with PIMT (ANOVA, $p < 0.0001$; Bonferroni's post-test $p < 0.01$ for H_2O_2 + Cp-ox/de *vs.* H_2O_2 + Cp-ox/de + *iso*DGR, $p < 0.0001$ for H_2O_2 + Cp-ox/de *vs.* H_2O_2 + Cp-ox/de + PIMT) (Fig. 9). Similarly, upon H_2O_2 + Cp-ox/de treatment, the amount of Cp bound to the cell monolayer,

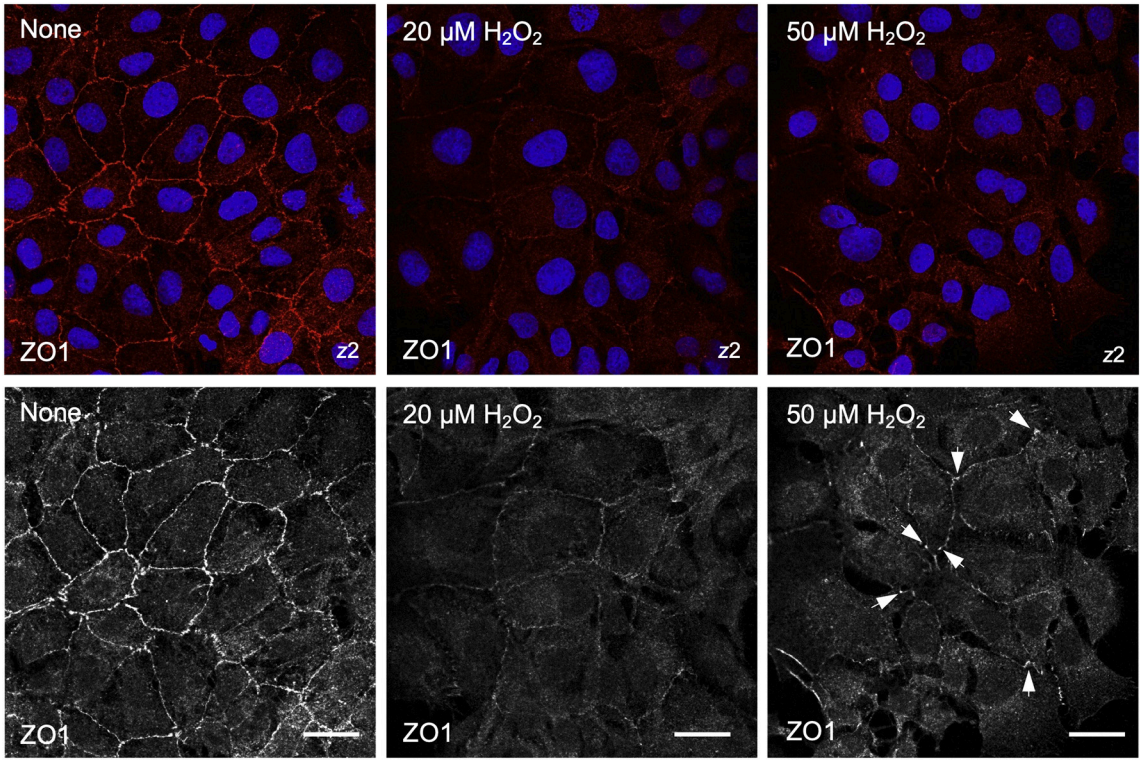

Fig. 7. Pathological oxidative environment induces tight junctions organization derangement. Expression and distribution of the ZO1 tight junctions protein marker was evaluated by immunofluorescence and confocal microscopy analysis in Z310 CPEpiCs monolayer upon treatment with H_2O_2 at concentrations corresponding to those detected in the CSF of either healthy subjects (20 μM) or Parkinson's disease patients (50 μM) (Barbariga et al., 2015). Upper panels show the ZO1 signal merged with Hoechest-33,342 nuclei staining; lower panels show ZO1 staining in gray levels mode. Arrows indicate the re-arranged dotted signal of ZO1 under pathological oxidative conditions. Bars = 25 μm. Brightness and contrast levels have been automatically adjusted on the entire images using Adobe Photoshop CS4 v11 software.

detectable in the cell lysates, was significantly higher than the Cp-ox/de bound upon treatment with Cp-ox/de alone (ANOVA, $p < 0.0001$; Bonferroni's post-test $p < 0.001$ for Cp-ox/de *vs.* H_2O_2 + Cp-ox/de) (Fig. 10a). The increase of Cp-ox/de binding to Z310 cells, observed upon the combined treatment, was reduced by both competition with *iso*DGR-peptide and Cp-ox/de pretreatment with PIMT (ANOVA, $p < 0.0001$; Bonferroni's post-test $p < 0.0001$ for H_2O_2 + Cp-ox/de *vs.* H_2O_2 + Cp-ox/de + *iso*DGR and $p < 0.01$ for H_2O_2 + Cp-ox/de *vs.* H_2O_2 + Cp-ox/de + PIMT) supporting the hypothesis of Cp-ox/de binding to RGD-recognizing integrins (presumably αVβ5 and α5β1) (Fig. 10a). Integrins engagement by Cp-ox/de under oxidative environment further worsened the choroid plexus barrier leakage induced by H_2O_2 treatment alone, while in the absence of oxidative environment Cp-ox/de was uneffective (Wilcoxon matched-pairs signed rank test: $p = 0.0497$, H_2O_2 *vs.* H_2O_2 + Cp-ox/de; $p = 0.0078$, None *vs.* H_2O_2; $p = 0.0156$, None *vs.* H_2O_2 + Cp-ox/de; p = ns, None *vs.* Cp-ox/de; p = 0.0078, for Cp-ox/de *vs.* H_2O_2 and *vs.* H_2O_2 + Cp-ox/de) (Fig. 10b).

The copper atoms coordinated within Cp molecule are released upon *in vitro* oxidation and deamidation (Barbariga et al., 2014). Even though free Cu atoms should not be present in the Cp-ox/de preparation because the modified protein was dialyzed before the use, to rule out any influence of Cu atoms on the observed Cp-ox/de effect on CPEpiCs barrier properties, we investigated the possible role that these atoms might exert on the CPEpiCs monolayer permeability. We used copper concentrations similar or higher than the theoretical concentration (about 800 nM) that can be achieved by the Cu atoms eventually released from the highest Cp concentration (20 μg/ml) used in the barrier permeability experiments. The results showed that the presence of the copper alone or in combination with oxidative conditions did not affect the barrier permeability properties of the choroid plexus epithelial cells (Fig. SM9).

Together, our results indicated that, under oxidative conditions, Cp-ox/de may cross the BCSFB, transducing an intracellular signal *via* integrin binding. This suggests that a pro-active interaction of Cp-ox/de with integrins may also occur *in vivo* in neurodegenerative pathologies characterized by oxidative stress.

4. Discussion

This work shows that RGD-recognizing integrins engagement by Cp-ox/de, *via* the *iso*DGR motif, triggers a signaling that alters CPEpiCs physiology in terms of cell proliferation, protein secretome profile, and BCSFB properties.

Asparagine deamidation is a spontaneous reaction that occurs during protein aging and that can be accelerated by the oxidative environment (Shimizu et al., 2005; Weintraub and Deverman, 2007). In the CSF of PD patients, the oxidative environment induces Cp deamidation at the ^{962}NGR motif, which is converted into the *iso*DGR-motif able to bind integrins (Barbariga et al., 2015, 2014; Olivieri et al., 2011; Zanardi and Alessio, 2021). Deamidation of the same NGR motif of Cp has been reported to occur in the serum of type 2 diabetes patients (Golizeh et al., 2017). Moreover, an enhanced deamidation of NGR motifs present in the ECM proteins has been reported in human atherosclerotic plaques, where the motif mediate monocyte adhesion *via* integrin binding (Dutta et al., 2017). Like the CSF of PD, the serum of diabetes patients and the atherosclerotic plaques are characterized by pro-oxidant pathological environments. Therefore, RGD-recognizing integrins engagement by deamidated NGR-motifs might be a mechanism of protein gain of function that occurs *in vivo* under pathological conditions implying oxidative stress. Whether the new function has favorable or detrimental consequences on the progression of the different pathologies is not yet known. Indeed, integrins engagement can result in the activation of different intracellular signaling, which regulates a plethora of events

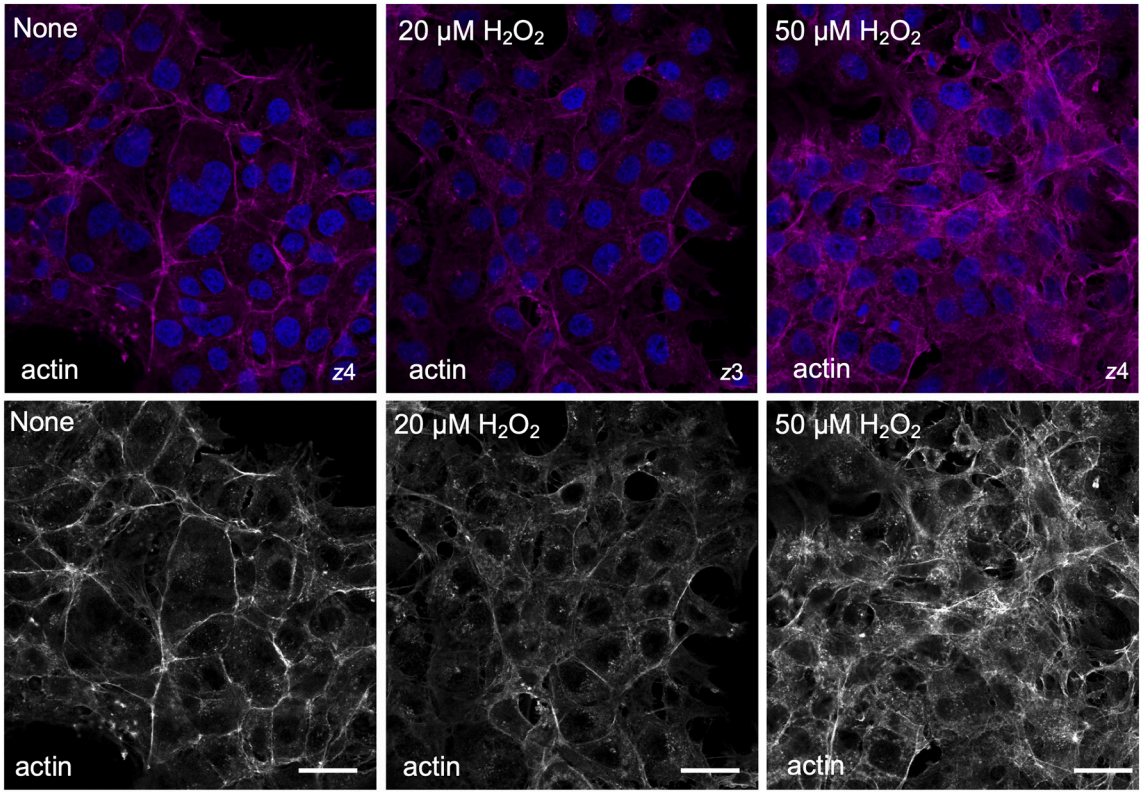

Fig. 8. Pathological oxidative environment promotes actin cytoskeleton disassembly. Expression and distribution of the actin fibers were evaluated by immunofluorescence and confocal microscopy analysis in Z310 CPEpiCs monolayer upon treatment with H_2O_2 at concentrations corresponding to those detected in the CSF of either healthy subjects (20 μM) or Parkinson's disease patients (50 μM) (Barbariga et al., 2015). Upper panels show the actin signal merged with Hoechest-33,342 nuclei staining; lower panels show actin staining in gray levels mode. Bars = 25 μm. Brightness and contrast levels have been automatically adjusted on the entire images using Adobe Photoshop CS4 v11 software.

such as cytoskeletal rearrangement, cell polarity, differentiation, growth, survival, and apoptosis (Gilmore, 2005; Lee and Streuli, 2014; Luo et al., 2007; Moreno-Layseca and Streuli, 2014; Streuli and Akhtar, 2009). In the case of Cp here described, it seems that the gain of RGD-recognizing integrins binding function is an unfavorable event that might progress the neurodegenerative conditions by altering the BCSFB features. Our hypothesis that CPEpiCs might be targeted by deamidated Cp found in the CSF of PD is supported by the evidence that, in both primary human CPEpiCs (Barbariga et al., 2020) and murine CPEpiC line, Cp-ox/de mediates cell adhesion and transduces a signaling that induces cell proliferation inhibition, *via isoDGR*/integrin binding. Differently from what was observed in epidermal epithelial cells (Barbariga et al., 2020), in CPEpiCs the proliferation inhibition mediated by Cp-ox/de does not result in overt apoptosis, but seems to be associated with the alteration of the cell-cell and cell-ECM interactions.

Our results show that Cp-ox/de directly compete for the binding of, at least α5β1, αVβ3 and αVβ5 integrins, and acts as antagonist for cells adhesion to both deamidated fibronectin module-5 and vitronectin. The information on inappropriate cell-matrix interaction is usually provided by integrins that sense the ECM and connect it to the cytoskeleton, transducing intracellular signals (Humphrey et al., 2014). Thus, it is conceivable that inappropriate RGD-recognizing integrins engagement by *iso*DGR motifs of Cp-ox/de might trigger a signal that alters CPEpiCs anchorage to basal lamina, leading to cell proliferation reduction. This type of signaling depends on 1) the kind of tissues/cells involved, which use different ECM components for the adhesion; 2) the different ECM-receptors expressed on the cells (*e.g.*, diverse integrins repertoire); 3) the pericellular proteolysis; and 4) the different co-stimulation provided by growth factor receptors signaling (Lee and Juliano, 2004; Michel, 2003). In the case of Cp-ox/de, anomalous signaling might be due, for example, to the interaction of integrins with a single molecule, rather than to the interaction with the physiologically organized ECM that usually leads to a multiple engagement and clustering of integrins in focal adhesion, a necessary event for an effective signaling transduction (Shattil et al., 2010). In alternative, the presence of two deamidated NGR motifs in the Cp sequence could lead to an inappropriate integrin dimerization which in in turn could lead to aberrant signaling.

Since we have shown that both NGR of Cp can undergo deamidation, resulting suitable for binding to RGD-recognizing integrins (Barbariga et al., 2014), a limitation of this study is the lack of identification of the specific role that these two Cp modification sites may play in the observed biological effects. In the future, it would be interesting to investigate this issue by using Cp mutants and synthetic peptides.

The integrins signaling also controls the secretion of growth factors and basal lamina components and the release of extracellular vesicles/exosomes, contributing to the changes of the extracellular milieu (Nolte et al., 2020). CPEpiCs have been reported to have high protein secretion capacity, their secretome, which also includes released microvesicles, mainly comprises carrier proteins, ECM-proteins, neurotrophic factors, proteases and protease inhibitors (Thouvenot et al., 2006). These proteins contribute to the homeostasis of the brain's extracellular environment and play a role in neuronal growth, differentiation and functions (Silva-Vargas et al., 2016). The proteins showing different levels of secretion we found in the CPEpiCs secretome represent the mentioned above groups of proteins and clearly indicated that Cp-ox/de affected these cells' physiology by interacting with integrins (at least α5β1, αVβ3 and αVβ5) and their interface with ECM, as inferred by competition experiments. The increased levels of collagen-IV-α1/−α5 and laminin-C1 found in the extracellular milieu upon Cp-ox/de treatment might result from the disassembly/derangement of the basal lamina and ECM anchorage of the CPEpiCs. This might be the consequence of the direct competition of Cp-ox/de with ECM proteins for the binding to RGD-

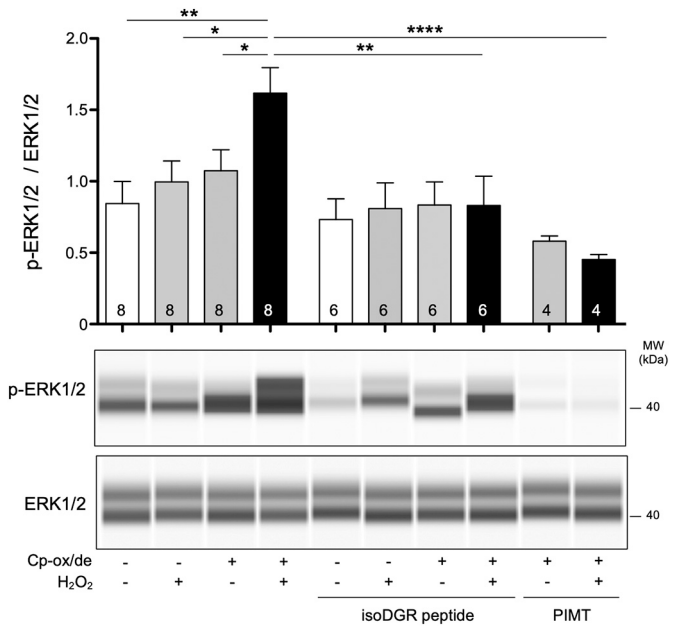

Fig. 9. Under oxidative conditions Cp-ox/de crosses the choroid plexus epithelial cell barrier, transducing an intracellular signal *via* integrin binding. Z310 CPEpiCs cell cultures on transwell system were treated 24 h with 50 μM H_2O_2 alone or 2 h with 20 μg/ml of Cp-ox/de alone, or with combined treatment H_2O_2 + Cp-ox/de. Cells were then washed and lysed. Protein extracts were used to evaluate by WB the expression and phosphorylation of ERK1/2. Competition to Cp-ox/de integrin binding was performed incubating cells with 30 μg/ml *iso*DGR-peptide 30 min before the addition of Cp-ox/de. Specificity of *iso*DGR-mediated integrin binding of Cp-ox/de was evaluated pre-treating Cp-ox/de with PIMT enzyme (16 h) before its addition to the CPEpiCs culture. Quantitative evaluation of the ratio of ERK1/2 phosphorylation and expression signals under different experimental conditions was performed by Simple Western capillary immunoassay on JESS system (ProteinSimple) using the ERK1/2 #9102 and p-Thr$^{202/}$Tyr^{204}ERK1/2 #9101 antibodies (Cell Signaling Technology). Protein expression levels and phosphorylation were quantified using the Compass software (ProteinSimple) and reported as ratio of p-ERK1/2: ERK1/2 signals. Representative cropped images of the ERK1/2 expression and phosphorylation (p-ERK1/2) signals obtained by Simple Western capillary immunoassay are shown. Statistical significance p value was evaluated by One-way ANOVA ($p = 0.0004$) comparing means ± SEM with Bonferroni's post-test analysis for comparison of selected pairs of groups (*, $p < 0.05$; **, $p < 0.01$; ***, $p < 0.001$; ****, $p < 0.0001$); number of biological replicates (n) is indicated within each bars of the different experimental conditions.

recognizing integrins as inferred by Cp-ox/de antagonism for cell binding to VN and deamidated FN-I_5. In the alternative, it could be the consequence of the signal transduced by inappropriate integrins engagement, which fosters the expression decrease of proteins necessary for the organization of ECM and basal lamina, like for example, the reduced levels found for the procollagen lysine hydroxylase (PLOD3), a protein in charge of collagen fibrils formation (Wang et al., 2009). In addition, the pericellular proteolysis could also be affected by the reduced levels of both SERPINE1 protease inhibitor and α-enolase, proteins involved in the ECM remodeling (Nakajima et al., 1994; Planus et al., 1997). In the case of semaphorin 7A, which contributes to focal adhesion formation and contains an RGD-integrin binding domain (Pasterkamp et al., 2003), a direct competition with Cp-ox/de for integrin binding might be conceivable.

From the molecular point of view, it is interesting to note that the signaling pathway transduced by the binding of Cp-ox/de to integrin in CPEpiCs, both HCPEpiCs (Barbariga et al., 2020) and Z310 cell line, is restricted to ERK1/2 activation, without the involvement of FAK1 and Akt. On the contrary, these kinases were activated in keratinocytes-derived epithelial cells by the same stimulus (Barbariga et al., 2014). This difference might explain why the apoptosis observed in HaCaT cells (Barbariga et al., 2020), was not induced in CPEpiCs. An integrin-mediated ERK1/2 activation has been reported to also occur independently from FAK activation, but itself is not sufficient to trigger mitogenic stimulus (Lee and Juliano, 2004). In order to induce cell proliferation, the cell adhesion mediated integrin signals need additional co-signaling events provided by growth factors *via* tyrosine kinase receptors (Lee and Juliano, 2004). Therefore, in the absence of FAK and Akt activation, the Cp-ox/de induced ERK1/2 phosphorylation should need one of such co-signaling stimuli to maintain cell proliferation. The absence or inadequate cross-talk between these signaling pathways might explain why CPEpiCs showed proliferation inhibition upon integrin engagement by Cp-ox/de. Noteworthy, a down-modulation of factors involved in cell growth and proliferation (such as α-enolase, insulin-like growth factor-binding protein 2, proliferation-associated protein 2G4, prosaposin) have been found among the proteins showing different levels in the secretome of HCPEpiCs treated with Cp-ox/de. This suggests an impoverishment in the CSF milieu of growth factors, which provide the co-signaling stimuli necessary for cell survival and/or proliferation, a condition that might be detrimental for many cells of the CNS, not only for CPEpiCs. In addition, an altered integrin-mediated signaling might also depend on the cellular integrin expression pattern, which can be modulated by the oxidative pathological environment (Lamari et al., 2007; Svineng et al., 2008), but this seems not to be the case in Z310 cells. Our results showed that Cp-ox/de interacts at least with α5β1 and αVβ3 integrins on HCPEpiCs, and with α5β1 and αVβ5 integrins on Z310 cells. However, even though we know that HCPEpiCs do not express αVβ5 and αVβ6 (Barbariga et al., 2020), and that Z310 cells do not express αVβ3, αVβ6 and αVβ8, we cannot exclude that other RGD-recognizing integrins (likely αVβ1, αVβ8 and α8β1) might be expressed by these cells and engaged by Cp-ox. The pattern of integrins expression and the role of individual integrins might explain different cellular responses to Cp-ox/de binding. For example, the observed limited spreading of Z310 cells on Cp-ox/de coated wells in comparison to HCPEpiCs and HaCaT cells, could be related to the lack of αVβ3 integrin expression. Indeed, it has been reported that αVβ3 in particular, more than other RGD-recognizing integrins, can stimulate Rac1 activity and extensive cell spreading, whereas α5β1 integrin mainly activates RhoA/ROCK pathways, which counteracts cell spreading promoting actin cytoskeletal rearrangement and cell motility (Danen et al., 2002; Lin et al., 2013; van der Bijl et al., 2020). The binding of FN to αVβ3 and α5β1 integrins promotes an antagonizing effect, rather than to act synergistically, and the different activation pathways seems to depend on the way of integrins interact with FN (αVβ3 binds only the RGD sites of FN, while α5β1 binds both the RGD sites and the synergy sites of FN) (van der Bijl et al., 2020). Thus, in the case of Cp-ox/de binding to α5β1 integrin, which is mediated only by *iso*DGR motifs, the transduced signaling might result to be inappropriate, limiting cytoskeletal rearrangement and cell proliferation. The dissection of the signal transduced by Cp-ox/de in the epithelial cells of the choroid plexus, in terms of RhoA/ROCK and/or Rac1 activation deserves to be investigated in the future.

Since integrins are usually expressed in the basolateral side of the CPEpiCs (Lee and Streuli, 2014), to transduce an anomalous integrin signaling, a mandatory condition was the possibility for Cp-ox/de, resident in the pathological CSF, to cross-back the BCSFB. Such condition is made possible by the BCSFB leakage promoted by the pro-oxidative CSF environment present in many neurodegenerative diseases. Indeed, it is documented that oxidative stress induces tight junction disruption in epithelial cells, affecting their barrier properties (Coisne and Engelhardt, 2011; Rao, 2008). Several oxidative compounds, including hydrogen peroxide, have been reported to disrupt adherens and tight junctions and their interaction with actin-cytoskeleton. This effect is mediated by the induction of protein modifications (oxidation, nitration and carbonylation), but also by modulating the intracellular signal transduction (Rao, 2008; Tietz and

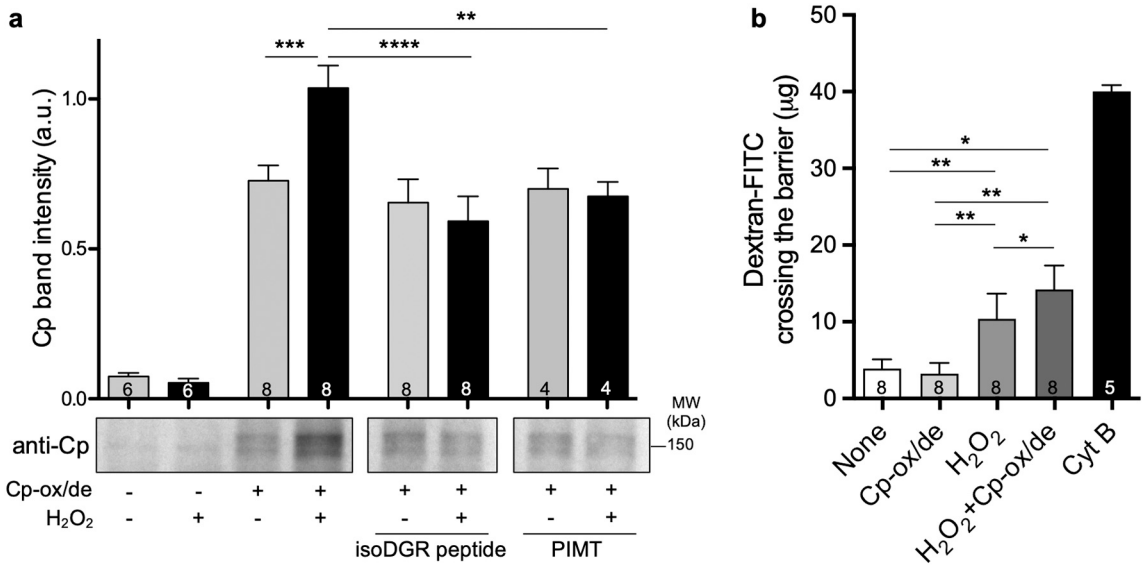

Fig. 10. Under oxidative conditions Cp-ox/de crosses the choroid plexus barrier and binds integrins, affecting barrier properties. Z310 cells cultured on transwell-system were treated with H_2O_2 (24 h, 50 µM) or with Cp-ox/de (2 h, 20 µg/ml), or with combined treatments (H_2O_2 + Cp-ox/de). Cells were washed and protein extracts were subjected to WB for cell-bound Cp quantification. Competition of Cp-ox/de binding was performed incubating the cells with an *iso*DGR-peptide (30 µg/ml) 30 min before the Cp-ox/de addition. Specificity of *iso*DGR-mediated integrin binding of Cp-ox/de was evaluated pre-treating Cp-ox/de with PIMT enzyme before the addition to CPEpiCs. **a)** Evaluation of Cp bound to Z310 CPEpiCs under different experimental conditions; signals were normalized to total proteins. Representative WB images of Cp-ox/de bound to the Z310 CPEpiCs are shown; cropped areas are from the same SDS-PAGE or twin gels, and same WB exposure. **b)** Z310 cells growing in transwell-systems were treated as described above, or 2 h with cytochalasin B (Cyt B) (1 µg/ml), and barrier permeability was measured evaluating the amount of dextran-FITC, dispensed in the upper chamber (100 µg), recovered in the lower chamber. Statistical significance p value was evaluated in panel A by One-way ANOVA ($p < 0.0001$) comparing means ± SEM with Bonferroni's post-test analysis; in panel B, due to the large variability in the biological replicates, the Wilcoxon matched-pairs signed rank test has been used to compare different treatments and controls within the same experiments. Number of biological replicates (n) is indicated within each bars of the different experimental conditions. *, $p < 0.05$; **, $p < 0.01$; ***, $p < 0.001$; ****, $p < 0.0001$.

Engelhardt, 2015). The observations that in the absence of an oxidative insult Cp-ox/de is neither able to cross the CPEpiCs monolayer nor to transduce an intracellular signaling, suggest that Cp-ox/de could contribute to PD as a secondary event of a multi-step pathological mechanism in which the alteration of BCSFB promoted by pro-oxidant factors, like hydrogen peroxide, is the primary event. We observed that the concentration of H_2O_2 necessary to induce both actin cytoskeleton and tight junctions derangement, which in turn foster barrier leakage, is comparable with the concentration detected in the CSF of PD patients (Barbariga et al., 2015); thus, induction of the BCSFB leakage is plausible to occur *in vivo* in patients. Indeed, alteration of the BCSFB has been reported to occur in advanced PD patients in which the oxidative stress might have acted for a long time (Pisani et al., 2012). Several other factors can contribute to the alteration/disruption of the BCSFB, for example, the dysfunctions in copper and iron homeostasis affect the BCSFB, favoring oxidative stress and degenerative protein modifications (Gallart-Palau et al., 2019; Marques et al., 2017; Mesquita et al., 2012; Zheng and Monnot, 2012). Cp, which coordinates 6 copper atoms, is one of the major Cu-transport proteins (Hellman and Gitlin, 2002), and the structural changes induced by aging or pro-oxidant pathological conditions, promote copper ions release (Barbariga et al., 2015, 2014; Musci et al., 1993; Olivieri et al., 2011; Sedlak et al., 2008). Thus, the amount of copper ions released in the CSF upon Cp oxidation could be pathologically relevant to BCSFB dysfunction, as reported for other barrier systems (Eskici and Axelsen, 2012; Ferruzza et al., 2002; Shukla et al., 2006). Nevertheless, the copper atoms concentration as possibly released from oxidized/deamidate Cp, under our experimental conditions, was not effective in altering CPEpiCs barrier properties. An additional consequence of Cp modifications and structural changes is the loss of ferroxidase activity, which favours intracellular iron accumulation and oxidative stress (Barbariga et al., 2015, 2014; Olivieri et al., 2011). This is underlined by the brain iron accumulation characterizing the rare genetic disease aceruloplasminemia (Piperno and Alessio, 2018). In the Cp knock-out mouse model of this disease, a strong iron deposition has been reported in the CPEpiCs (Zanardi et al., 2018), thus it is plausible that BCSFB leakage might be induced/strengthen by iron-mediated intracellular oxidative stress.

The more relevant finding is that once crossed the barrier thanks to the BCSFB leakage fostered by the oxidative environment, the Cp-ox/de can bind RGD-recognizing integrins and transduce an intracellular signal that worse the CPEpiCs barrier alteration. This aggravation could result from several factors: 1) the signal activation limited to ERK1/2, which has been reported to play a major role in hydrogen peroxide-induced disruption of barrier function in brain endothelial cell monolayer (Kevil et al., 2001; Rao, 2008); 2) the inhibition of CPEpiCs proliferation, that could contribute to the barrier impairment altering the physiological epithelial cells turnover necessary to maintain monolayer homeostasis (Barkho and Monuki, 2015); 3) the direct competition that Cp-ox/de might have with the ECM for the binding to integrins, which could alter tensegrity signaling affecting both epithelial cells' polarity and barrier organization (Lee and Streuli, 2014).

Interestingly, different RGD-binding integrins, in particular αVβ3 and α5β1, have distinct effects on cell-cell junction formation and barrier function in epithelial and endothelial cells. This is, at least in part, due to differences in the activation of Rac and RhoA. Indeed the α5β1 integrin activation, throughout the RhoA/ROCK pathway, promotes actin cytoskeletal rearrangement and regulates cadherin expression which in turn favours the disassembly cell-cell junction, and barrier leakage in endothelial cells (Amado-Azevedo et al., 2021; Hakanpaa et al., 2018, 2015; van der Bijl et al., 2020). On the opposite, the lack of αVβ3 integrin engagement, which is mainly involved in focal adhesion structures, and the consequent fail of downstream Rac1 activation promotes vascular leakage (Su et al., 2012).

Regarding the αVβ5 integrin engagement by Cp-ox/de, it has been reported that, in addition to be recruited in focal adhesion for VN binding, αVβ5 is a phagocytic integrin which is abundantly found in

clathrin-coated structures and flat clathrin lattices, mechanotransduction structures that sense the cell substrate stiffness independently from actin cytoskeletal contractility (Baschieri et al., 2018; Zuidema et al., 2018). Similar role has the location of αVβ5 in the reticular adhesion complexes, which maintain cell-ECM attachment during cell division in the absence of actin cytoskeletal fibers organization (Lock et al., 2018). Interestingly, the β5 staining we observed in Z310 cells is reminiscent of such clathrin pits/lattices and reticular adhesion structures, suggesting that Cp-ox/de, interfering with them by competition to VN binding, might alter both mechanotransduction signaling and adhesion to the basal lamina, affecting cell division/proliferation.

5. Conclusions

The loss of ferroxidase activity and the gain of RGD-recognizing integrin binding function of Cp, as a consequence of the modifications induced in the pathological PD CSF environment, might contribute to the mechanisms of neurodegeneration affecting CPEpiCs physiology. This alteration is added to the already present BCSFB leakage promoted by the oxidative stress conditions and worsens the choroid plexus barrier properties. The interaction of Cp-ox/de with RGD-recognizing integrins on the surface of CPEpiCs, affects the barrier modifying likely the interaction of cells with the ECM, antagonizing the binding to VN and deamidated fibronectin, and limiting cell monolayer renewal. Furthermore, the cross-talk between CPEpiCs and the other CNS cells, mediated by exosomes and secreted proteins, is also affected. Together these circumstances represent a novel mechanism with potentially critical pathological implications in PD that might contribute to neurodegeneration, not only at the level of CPEpiCs barrier, but also in a scenario within the CNS that involves other cells expressing suitable integrins and/or that are susceptible to oxidative stress.

Data availability

The datasets used and/or analyzed during the current study are available from the corresponding author on reasonable request.

Funding

This research did not receive any specific grant from funding agencies in the public, commercial, or not-for-profit sectors.

Authors' information

Alan Zanardi is a recipient of a fellowship from Fondazione Centro San Raffaele, Milano, Italy. Franco Vegliani was an Erasmus-Traineeships from University of Glasgow (current address: Institute of Molecular, Cell and Systems Biology, University of Glasgow, Glasgow, UK).

Declaration of Competing Interest

Authors declare that they have no competing financial interests.

Acknowledgments

MA is supported by Italian Ministry of Health (RF-2018-12366471). We thank the Advanced Light and Electron Microscopy BioImaging Center at San Raffaele Hospital for confocal microscopy assistance. Z310 cell line was kindly provided by Dr. W. Zheng, Purdue University, West Lafayette, IN.

Appendix A. Supplementary data

Supplementary data to this article can be found online at https://doi.org/10.1016/j.nbd.2021.105474.

References

Amado-Azevedo, J., van Stalborch, A.-M.D., Valent, E.T., Nawaz, K., van Bezu, J., Eringa, E.C., Hoevenaars, F.P.M., De Cuyper, I.M., Hordijk, P.L., van Hinsbergh, V. W.M., van Nieuw Amerongen, G.P., Aman, J., Margadant, C., 2021. Depletion of Arg/Abl2 improves endothelial cell adhesion and prevents vascular leak during inflammation. Angiogenesis. https://doi.org/10.1007/s10456-021-09781-x.

Anthony, S.G., Schipper, H.M., Tavares, R., Hovanesian, V., Cortez, S.C., Stopa, E.G., Johanson, C.E., 2003. Stress protein expression in the Alzheimer-diseased choroid plexus. J. Alzheimers Dis. 5, 171–177.

Ayton, S., Lei, P., Duce, J.A., Wong, B.X., Sedjahtera, A., Adlard, P.A., Bush, A.I., Finkelstein, D.I., 2013. Ceruloplasmin dysfunction and therapeutic potential for parkinson disease. Ann. Neurol. 73, 554–559. https://doi.org/10.1002/ana.23817.

Balusu, S., Van Wonterghem, E., De Rycke, R., Raemdonck, K., Stremersch, S., Gevaert, K., Brkic, M., Demeestere, D., Vanhooren, V., Hendrix, A., Libert, C., Vandenbroucke, R.E., 2016. Identification of a novel mechanism of blood-brain communication during peripheral inflammation via choroid plexus-derived extracellular vesicles. EMBO Mol. Med. 8, 1162–1183. Doi:10.15252/emmm.201606271.

Barbariga, M., Curnis, F., Spitaleri, A., Andolfo, A., Zucchelli, C., Lazzaro, M., Magnani, G., Musco, G., Corti, A., Alessio, M., 2014. Oxidation-induced structural changes of Ceruloplasmin Foster NGR motif Deamidation that promotes integrin binding and signaling. J. Biol. Chem. 289, 3736–3748. https://doi.org/10.1074/jbc.M113.520981.

Barbariga, M., Curnis, F., Andolfo, A., Zanardi, A., Lazzaro, M., Conti, A., Magnani, G., Volontè, M.A., Ferrari, L., Comi, G., Corti, A., Alessio, M., 2015. Ceruloplasmin functional changes in Parkinson's disease-cerebrospinal fluid. Mol. Neurodegener. 10, 59. https://doi.org/10.1186/s13024-015-0055-2.

Barbariga, M., Zanardi, A., Curnis, F., Conti, A., Boselli, D., Di Terlizzi, S., Alessio, M., 2020. Ceruloplasmin oxidized and deamidated by Parkinson's disease cerebrospinal fluid induces epithelial cells proliferation arrest and apoptosis. Sci. Rep. 10, 15507. https://doi.org/10.1038/s41598-020-72447-z.

Barkho, B.Z., Monuki, E.S., 2015. Proliferation of cultured mouse choroid plexus epithelial cells. PLoS One 10, e0121738. https://doi.org/10.1371/journal.pone.0121738.

Baschieri, F., Dayot, S., Elkhatib, N., Ly, N., Capmany, A., Schauer, K., Betz, T., Vignjevic, D.M., Poincloux, R., Montagnac, G., 2018. Frustrated endocytosis controls contractility-independent mechanotransduction at clathrin-coated structures. Nat. Commun. 9, 3825. https://doi.org/10.1038/s41467-018-06367-y.

van der Bijl, I., Nawaz, K., Kazlauskaite, U., van Stalborch, A.-M., Tol, S., Jimenez Orgaz, A., van den Bout, I., Reinhard, N.R., Sonnenberg, A., Margadant, C., 2020. Reciprocal integrin/integrin antagonism through kindlin-2 and rho GTPases regulates cell cohesion and collective migration. Matrix Biol. 93, 60–78. https://doi.org/10.1016/j.matbio.2020.05.005.

Borst, A.J., James, Z.M., Zagotta, W.N., Ginsberg, M., Rey, F.A., DiMaio, F., Backovic, M., Veesler, D., 2017. The therapeutic antibody LM609 selectively inhibits ligand binding to human αVβ3 integrin via steric hindrance. Structure 25. https://doi.org/10.1016/j.str.2017.09.007, 1732-1739.e5.

Brkic, M., Balusu, S., Van Wonterghem, E., Gorle, N., Benilova, I., Kremer, A., Van Hove, I., Moons, L., De Strooper, B., Kanazir, S., Libert, C., Vandenbroucke, R.E., 2015. Amyloid beta oligomers disrupt blood-CSF barrier integrity by activating matrix Metalloproteinases. J. Neurosci. 35, 12766–12778. https://doi.org/10.1523/JNEUROSCI.0006-15.2015.

Coisne, C., Engelhardt, B., 2011. Tight junctions in brain barriers during central nervous system inflammation. Antioxid. Redox Signal. 15, 1285–1303. https://doi.org/10.1089/ars.2011.3929.

Corti, A., Curnis, F., 2011. Isoaspartate-dependent molecular switches for integrin-ligand recognition. J. Cell Sci. 124, 515–522. https://doi.org/10.1242/jcs.077172 124/4/515 (pii).

Curnis, F., Longhi, R., Crippa, L., Cattaneo, A., Dondossola, E., Bachi, A., Corti, A., 2006. Spontaneous formation of L-isoaspartate and gain of function in fibronectin. J. Biol. Chem. 281, 36466–36476 doi:M604812200 [pii]. https://doi.org/10.1074/jbc.M604812200.

Danen, E.H.J., Sonneveld, P., Brakebusch, C., Fässler, R., Sonnenberg, A., 2002. The fibronectin-binding integrins α5β1 and αvβ3 differentially modulate RhoA–GTP loading, organization of cell matrix adhesions, and fibronectin fibrillogenesis. J. Cell Biol. 159, 1071–1086. https://doi.org/10.1083/jcb.200205014.

Demeestere, D., Libert, C., Vandenbroucke, R.E., 2015. Clinical implications of leukocyte infiltration at the choroid plexus in (neuro)inflammatory disorders. Drug Discov. Today 20, 928–941. https://doi.org/10.1016/j.drudis.2015.05.003.

Dutta, B., Park, J.E., Kumar, S., Hao, P., Gallart-Palau, X., Serra, A., Ren, Y., Sorokin, V., Lee, C.N., Ho, H.H., de Kleijn, D., Sze, S.K., 2017. Monocyte adhesion to atherosclerotic matrix proteins is enhanced by Asn-Gly-Arg deamidation. Sci. Rep. 7, 5765. https://doi.org/10.1038/s41598-017-06202-2.

Emerich, D.F., Skinner, S.J., Borlongan, C.V., Vasconcellos, A.V., Thanos, C.G., 2005. The choroid plexus in the rise, fall and repair of the brain. Bioessays 27, 262–274. https://doi.org/10.1002/bies.20193.

Eskici, G., Axelsen, P.H., 2012. Copper and oxidative stress in the pathogenesis of Alzheimer's disease. Biochemistry 51, 6289–6311. https://doi.org/10.1021/bi3006169.

Ferruzza, S., Scacchi, M., Scarino, M.L., Sambuy, Y., 2002. Iron and copper alter tight junction permeability in human intestinal Caco-2 cells by distinct mechanisms. Toxicol. in Vitro 16, 399–404. https://doi.org/10.1016/s0887-2333(02)00020-6.

Gallart-Palau, X., Tan, L.M., Serra, A., Gao, Y., Ho, H.H., Richards, A.M., Kandiah, N., Chen, C.P., Kalaria, R.N., Sze, S.K., 2019. Degenerative protein modifications in the aging vasculature and central nervous system: a problem shared is not always halved. Ageing Res. Rev. 53, 100909. https://doi.org/10.1016/j.arr.2019.100909.
Gilmore, A.P., 2005. Anoikis. Cell Death Differ. 12 (Suppl. 2), 1473–1477. https://doi.org/10.1038/sj.cdd.4401723.
Golizeh, M., Lee, K., Ilchenko, S., Osme, A., Bena, J., Sadygov, R.G., Kashyap, S.R., Kasumov, T., 2017. Increased serotransferrin and ceruloplasmin turnover in diet-controlled patients with type 2 diabetes. Free Radic. Biol. Med. 113, 461–469. https://doi.org/10.1016/j.freeradbiomed.2017.10.373.
Grapp, M., Wrede, A., Schweizer, M., Huwel, S., Galla, H.J., Snaidero, N., Simons, M., Buckers, J., Low, P.S., Urlaub, H., Gartner, J., Steinfeld, R., 2013. Choroid plexus transcytosis and exosome shuttling deliver folate into brain parenchyma. Nat. Commun. 4, 2123. https://doi.org/10.1038/ncomms3123.
Hakanpaa, L., Sipila, T., Leppanen, V.-M., Gautam, P., Nurmi, H., Jacquemet, G., Eklund, L., Ivaska, J., Alitalo, K., Saharinen, P., 2015. Endothelial destabilization by angiopoietin-2 via integrin β1 activation. Nat. Commun. 6, 5962. https://doi.org/10.1038/ncomms6962.
Hakanpaa, L., Kiss, E.A., Jacquemet, G., Miinalainen, I., Lerche, M., Guzmán, C., Mervaala, E., Eklund, L., Ivaska, J., Saharinen, P., 2018. Targeting β1-integrin inhibits vascular leakage in endotoxemia. Proc. Natl. Acad. Sci. U. S. A. 115, E6467–E6476. https://doi.org/10.1073/pnas.1722317115.
Hellman, N.E., Gitlin, J.D., 2002. Ceruloplasmin metabolism and function. Annu. Rev. Nutr. 22, 439–458. https://doi.org/10.1146/annurev.nutr.22.012502.114457 (012502.114457 [pii]).
Humphrey, J.D., Dufresne, E.R., Schwartz, M.A., 2014. Mechanotransduction and extracellular matrix homeostasis. Nat. Rev. Mol. Cell Biol. 15, 802–812. https://doi.org/10.1038/nrm3896.
Jeong, S.Y., David, S., 2003. Glycosylphosphatidylinositol-anchored ceruloplasmin is required for iron efflux from cells in the central nervous system. J. Biol. Chem. 278, 27144–27148. https://doi.org/10.1074/jbc.M301988200 (M301988200 [pii]).
Johanson, C.E., Stopa, E.G., McMillan, P.N., 2011. The blood-cerebrospinal fluid barrier: structure and functional significance. Methods Mol. Biol. 686, 101–131. https://doi.org/10.1007/978-1-60761-938-3_4.
Kaur, C., Rathnasamy, G., Ling, E.A., 2016. The choroid plexus in healthy and diseased brain. J. Neuropathol. Exp. Neurol. 75, 198–213. https://doi.org/10.1093/jnen/nlv030.
Kevil, C.G., Okayama, N., Alexander, J.S., 2001. H_2O_2-mediated permeability II: importance of tyrosine phosphatase and kinase activity. Am. J. Phys. Cell Phys. 281, C1940–C1947. https://doi.org/10.1152/ajpcell.2001.281.6.C1940.
Lamari, F., Braut-Boucher, F., Pongnimitprasert, N., Bernard, M., Foglietti, M.-J., Derappe, C., Aubery, M., 2007. Cell adhesion and integrin expression are modulated by oxidative stress in EA.hy 926 cells. Free Radic. Res. 41, 812–822. https://doi.org/10.1080/10715760701390027.
Lee, J.L., Streuli, C.H., 2014. Integrins and epithelial cell polarity. J. Cell Sci. 127, 3217–3225. https://doi.org/10.1242/jcs.146142.
Lee, J.W., Juliano, R., 2004. Mitogenic signal transduction by integrin- and growth factor receptor-mediated pathways. Mol. Cell 17, 188–202.
Lin, G.L., Cohen, D.M., Desai, R.A., Breckenridge, M.T., Gao, L., Humphries, M.J., Chen, C.S., 2013. Activation of beta 1 but not beta 3 integrin increases cell traction forces. FEBS Lett. 587, 763–769. https://doi.org/10.1016/j.febslet.2013.01.068.
Lock, J.G., Jones, M.C., Askari, J.A., Gong, X., Oddone, A., Olofsson, H., Göransson, S., Lakadamyali, M., Humphries, M.J., Strömblad, S., 2018. Reticular adhesions are a distinct class of cell-matrix adhesions that mediate attachment during mitosis. Nat. Cell Biol. 20, 1290–1302. https://doi.org/10.1038/s41556-018-0220-2.
Luo, B.H., Carman, C.V., Springer, T.A., 2007. Structural basis of integrin regulation and signaling. Annu. Rev. Immunol. 25, 619–647. https://doi.org/10.1146/annurev.immunol.25.022106.141618.
Marques, F., Sousa, J.C., Brito, M.A., Pahnke, J., Santos, C., Correia-Neves, M., Palha, J. A., 2017. The choroid plexus in health and in disease: dialogues into and out of the brain. Neurobiol. Dis. 107, 32–40. https://doi.org/10.1016/j.nbd.2016.08.011.
Masseguin, C., LePanse, S., Corman, B., Verbavatz, J.M., Gabrion, J., 2005. Aging affects choroidal proteins involved in CSF production in Sprague-Dawley rats. Neurobiol. Aging 26, 917–927. https://doi.org/10.1016/j.neurobiolaging.2004.07.013.
Mesquita, S.D., Ferreira, A.C., Sousa, J.C., Santos, N.C., Correia-Neves, M., Sousa, N., Palha, J.A., Marques, F., 2012. Modulation of iron metabolism in aging and in Alzheimer's disease: relevance of the choroid plexus. Front. Cell. Neurosci. 6, 25. https://doi.org/10.3389/fncel.2012.00025.
Michel, J.B., 2003. Anoikis in the cardiovascular system: known and unknown extracellular mediators. Arterioscler. Thromb. Vasc. Biol. 23, 2146–2154. https://doi.org/10.1161/01.ATV.0000099882.52647.E4.
Monnot, A.D., Zheng, W., 2013. Culture of choroid plexus epithelial cells and in vitro model of blood-CSF barrier. Methods Mol. Biol. 945, 13–29. https://doi.org/10.1007/978-1-62703-125-7_2.
Moreno-Layseca, P., Streuli, C.H., 2014. Signalling pathways linking integrins with cell cycle progression. Matrix Biol. 34, 144–153. https://doi.org/10.1016/j.matbio.2013.10.011.
Mould, A.P., Askari, J.A., Aota, S., Yamada, K.M., Irie, A., Takada, Y., Mardon, H.J., Humphries, M.J., 1997. Defining the topology of integrin α5β1-Fibronectin interactions using inhibitory anti-α5 and anti-β1 monoclonal antibodies. J. Biol. Chem. 272, 17283–17292. https://doi.org/10.1074/jbc.272.28.17283.
Musci, G., Bonaccorsi di Patti, M.C., Fagiolo, U., Calabrese, L., 1993. Age-related changes in human ceruloplasmin. Evidence for oxidative modifications. J. Biol. Chem. 268, 13388–13395.
Nakajima, K., Hamanoue, M., Takemoto, N., Hattori, T., Kato, K., Kohsaka, S., 1994. Plasminogen binds specifically to alpha-enolase on rat neuronal plasma membrane. J. Neurochem. 63, 2048–2057. https://doi.org/10.1046/j.1471-4159.1994.63062048.x.
Nolte, M.A., Nolte-'t Hoen, E.N.M., Margadant, C., 2020. Integrins control vesicular trafficking; New tricks for old dogs. Trends Biochem. Sci. https://doi.org/10.1016/j.tibs.2020.09.001. S0968000420302267.
Olivieri, S., Conti, A., Iannaccone, S., Cannistraci, C.V., Campanella, A., Barbariga, M., Codazzi, F., Pelizzoni, I., Magnani, G., Pesca, M., Franciotta, D., Cappa, S.F., Alessio, M., 2011. Ceruloplasmin oxidation, a feature of Parkinson's disease CSF, inhibits ferroxidase activity and promotes cellular iron retention. J. Neurosci. 31, 18568–18577. https://doi.org/10.1523/JNEUROSCI.3768-11.2011.
Pasterkamp, R.J., Peschon, J.J., Spriggs, M.K., Kolodkin, A.L., 2003. Semaphorin 7A promotes axon outgrowth through integrins and MAPKs. Nature 424, 398–405. https://doi.org/10.1038/nature01790.
Perez-Gracia, E., Blanco, R., Carmona, M., Carro, E., Ferrer, I., 2009. Oxidative stress damage and oxidative stress responses in the choroid plexus in Alzheimer's disease. Acta Neuropathol. 118, 497–504. https://doi.org/10.1007/s00401-009-0574-4.
Piperno, A., Alessio, M., 2018. Aceruloplasminemia: waiting for an efficient therapy. Front. Neurosci. 12, 903. https://doi.org/10.3389/fnins.2018.00903.
Pisani, V., Stefani, A., Pierantozzi, M., Natoli, S., Stanzione, P., Franciotta, D., Pisani, A., 2012. Increased blood-cerebrospinal fluid transfer of albumin in advanced Parkinson's disease. J. Neuroinflammation 9, 188. https://doi.org/10.1186/1742-2094-9-188.
Planus, E., Barlovatz-Meimon, G., Rogers, R.A., Bonavaud, S., Ingber, D.E., Wang, N., 1997. Binding of urokinase to plasminogen activator inhibitor type-1 mediates cell adhesion and spreading. J. Cell Sci. 110 (Pt 9), 1091–1098.
Rao, R., 2008. Oxidative stress-induced disruption of epithelial and endothelial tight junctions. Front. Biosci. 7210. https://doi.org/10.2741/3223.
Redzic, Z.B., 2013. Studies on the human choroid plexus in vitro. Fluids Barriers CNS 10, 10. https://doi.org/10.1186/2045-8118-10-10 (2045-8118-10-10 [pii]).
Romero-Calvo, I., Ocón, B., Martínez-Moya, P., Suárez, M.D., Zarzuelo, A., Martínez-Augustin, O., de Medina, F.S., 2010. Reversible Ponceau staining as a loading control alternative to actin in Western blots. Anal. Biochem. 401, 318–320. https://doi.org/10.1016/j.ab.2010.02.036.
Sedlak, E., Zoldak, G., Wittung-Stafshede, P., 2008. Role of copper in thermal stability of human ceruloplasmin. Biophys. J. 94, 1384–1391 doi:S0006-3495(08)70655-6 [pii]. https://doi.org/10.1529/biophysj.107.113696.
Serot, J.M., Bene, M.C., Foliguet, B., Faure, G.C., 1997. Altered choroid plexus basement membrane and epithelium in late-onset Alzheimer's disease: an ultrastructural study. Ann. N. Y. Acad. Sci. 826, 507–509.
Shattil, S.J., Kim, C., Ginsberg, M.H., 2010. The final steps of integrin activation: the end game. Nat. Rev. Mol. Cell Biol. 11, 288–300. https://doi.org/10.1038/nrm2871.
Shimizu, T., Matsuoka, Y., Shirasawa, T., 2005. Biological significance of isoaspartate and its repair system. Biol. Pharm. Bull. 28, 1590–1596 (Doi:JST.JSTAGE/bpb/28.1590 pii).
Shrestha, B., Paul, D., Pachter, J.S., 2014. Alterations in tight junction protein and IgG permeability accompany leukocyte extravasation across the choroid plexus during neuroinflammation. J. Neuropathol. Exp. Neurol. 73, 1047–1061. https://doi.org/10.1097/NEN.0000000000000127.
Shukla, N., Maher, J., Masters, J., Angelini, G.D., Jeremy, J.Y., 2006. Does oxidative stress change ceruloplasmin from a protective to a vasculopathic factor? Atherosclerosis 187, 238–250. https://doi.org/10.1016/j.atherosclerosis.2005.11.035.
Silva-Vargas, V., Maldonado-Soto, A.R., Mizrak, D., Codega, P., Doetsch, F., 2016. Age-dependent niche signals from the choroid plexus regulate adult neural stem cells. Cell Stem Cell 19, 643–652. https://doi.org/10.1016/j.stem.2016.06.013.
Streuli, C.H., Akhtar, N., 2009. Signal co-operation between integrins and other receptor systems. Biochem. J. 418, 491–506. https://doi.org/10.1042/BJ20081948.
Su, G., Atakilit, A., Li, J.T., Wu, N., Bhattacharya, M., Zhu, J., Shieh, J.E., Li, E., Chen, R., Sun, S., Su, C.P., Sheppard, D., 2012. Absence of integrin αvβ3 enhances vascular leak in mice by inhibiting endothelial cortical actin formation. Am. J. Respir. Crit. Care Med. 185, 58–66. https://doi.org/10.1164/rccm.201108-1381OC.
Svineng, G., Ravuri, C., Rikardsen, O., Huseby, N.E., Winberg, J.O., 2008. The role of reactive oxygen species in integrin and matrix metalloproteinase expression and function. Connect. Tissue Res. 49, 197–202. https://doi.org/10.1080/03008200802143166 (795330911 [pii]).
Texel, S.J., Xu, X., Harris, Z.L., 2008. Ceruloplasmin in neurodegenerative diseases. Biochem. Soc. Trans. 36, 1277–1281. https://doi.org/10.1042/BST0361277 (BST0361277 [pii]).
Thouvenot, E., Lafon-Cazal, M., Demettre, E., Jouin, P., Bockaert, J., Marin, P., 2006. The proteomic analysis of mouse choroid plexus secretome reveals a high protein secretion capacity of choroidal epithelial cells. Proteomics 6, 5941–5952. https://doi.org/10.1002/pmic.200600096.
Tietz, S., Engelhardt, B., 2015. Brain barriers: crosstalk between complex tight junctions and adherens junctions. J. Cell Biol. 209, 493–506. https://doi.org/10.1083/jcb.201412147.
Vargas, T., Ugalde, C., Spuch, C., Antequera, D., Moran, M.J., Martin, M.A., Ferrer, I., Bermejo-Pareja, F., Carro, E., 2010. Abeta accumulation in choroid plexus is associated with mitochondrial-induced apoptosis. Neurobiol. Aging 31, 1569–1581. https://doi.org/10.1016/j.neurobiolaging.2008.08.017.
Wang, C., Kovanen, V., Raudasoja, P., Eskelinen, S., Pospiech, H., Myllyla, R., 2009. The glycosyltransferase activities of lysyl hydroxylase 3 (LH3) in the extracellular space are important for cell growth and viability. J. Cell. Mol. Med. 13, 508–521. https://doi.org/10.1111/j.1582-4934.2008.00286.x.
Weintraub, S.J., Deverman, B.E., 2007. Chronoregulation by asparagine deamidation. Sci. STKE 2007, re7 doi:stke.4092007re7 [pii]. https://doi.org/10.1126/stke.4092007re7.

Zanardi, A., Alessio, M., 2021. Ceruloplasmin Deamidation in Neurodegeneration: from loss to gain of function. IJMS 22, 663. https://doi.org/10.3390/ijms22020663.
Zanardi, A., Conti, A., Cremonesi, M., D'Adamo, P., Gilberti, E., Apostoli, P., Cannistraci, C.V., Piperno, A., David, S., Alessio, M., 2018. Ceruloplasmin replacement therapy ameliorates neurological symptoms in a preclinical model of aceruloplasminemia. EMBO Mol. Med. 10, 91–106. Doi:10.15252/emmm.201708361.
Zheng, W., Monnot, A.D., 2012. Regulation of brain iron and copper homeostasis by brain barrier systems: implication in neurodegenerative diseases. Pharmacol. Ther. 133, 177–188. https://doi.org/10.1016/j.pharmthera.2011.10.006.
Zheng, W., Zhao, Q., 2002. Establishment and characterization of an immortalized Z310 choroidal epithelial cell line from murine choroid plexus. Brain Res. 958, 371–380.
Zuidema, A., Wang, W., Kreft, M., te Molder, L., Hoekman, L., Bleijerveld, O.B., Nahidiaza, L., Janssen, H., Sonnenberg, A., 2018. Mechanisms of integrin αVβ5 clustering in flat clathrin lattices (preprint). Cell Biology. https://doi.org/10.1101/427112.